Mechanical Systems and Signal Processing 88 (2017) 253–273

Contents lists available at ScienceDirect

Mechanical Systems and Signal Processing

journal homepage: www.elsevier.com/locate/ymssp

Review

A spectral approach for damage quantification in stochastic dynamic systems

M.R. Machado[a,*], S. Adhikari[b], J.M.C. Dos Santos[a]

[a] University of Campinas, UNICAMP-FEM-DMC, Rua Mendeleyev, 200, CEP 13083-970 Campinas, SP, Brazil
[b] Swansea University, Singleton Park, Swansea SA2 8PP, UK

ARTICLE INFO

Keywords:
Damage detection
Uncertainties quantification
Random field
Inverse problem

ABSTRACT

Intrinsic to all real structures, parameter uncertainty can be found in material properties and geometries. Many structural parameters, such as, elastic modulus, Poisson's rate, thickness, density, etc., are spatially distributed by nature. The Karhunen-Loève expansion is a method used to model the random field expanded in a spectral decomposition. Once many structural parameters can not be modelled as a Gaussian distribution the memoryless nonlinear transformation is used to translate a Gaussian random field in a non-Gaussian. Thus, stochastic methods have been used to include these uncertainties in the structural model. The Spectral Element Method (SEM) is a wave-based numerical approach used to model structures. It is also developed to express parameters as spatially correlated random field in its formulation. In this paper, the problem of structural damage detection under the presence of spatially distributed random parameter is addressed. Explicit equations to localize and assess damage are proposed based on the SEM formulation. Numerical examples in an axially vibrating undamaged and damaged structure with distributed parameters are analysed.

1. Introduction

In general, changes in either global or local structural properties can be associated with damage parameters. Over the last decades, many works have been performed to develop vibration-based non-destructive evaluation (NDE) methods, which allow a damage to be localised and quantified from modal parameters and dynamic response [1,2]. However, these techniques are well suited to detect large rather than small damages like a crack. Structural crack does not impose appreciable changes at low-frequency and the global structural behaviour is unaffected. The presence of a crack in a structure introduces local flexibility that affects its vibration response. It also generates changes in the elastic waves that propagate in the structure. New and recent researches about damage quantification are concentrated on methods that use elastic wave propagation in structures at medium and high frequencies [3–7]. They use the inherent material property that discontinuities, such as a crack, generate changes in the elastic waves propagating in the structure. There are some particular advantages of elastic wave-based damage quantification, such as their capacity to propagate over significant distances and high sensitivity to discontinuities near the wave propagation path.

The spectral element method (SEM) [8,9] is based on the analytical solution of the displacement wave equation, written in the frequency domain. The element is tailored with the matrix ideas of the finite element method (FEM), where the interpolation function is the exact solution of wave equation. This approach has been called by different names, such as the dynamic stiffness method [10–20], spectral finite element method [21,22] and dynamic finite element method [23,24]. Built-up structures with

* Corresponding author.
E-mail address: mrmomarcela@gmail.com (M.R. Machado).

http://dx.doi.org/10.1016/j.ymssp.2016.11.018
Received 20 June 2016; Received in revised form 31 October 2016; Accepted 19 November 2016
Available online 01 December 2016

geometrically uniform members can be modelled by a single spectral element. This can reduce significantly the total number of degrees of freedom compared to other similar methods.

Since the method is based on the wave equation it performs well at medium and high-frequency bands. However, there are still some drawbacks, such as difficulties to model non-uniform members and to apply arbitrary boundary conditions for 2D and 3D elements. Although SEM ensures exact frequency-domain it is not true for time-domain solutions, which are largely used for damage detection studies. Errors due to aliasing or leakage are predictable in the use of the inverse Discret Fourier Transform (DFT) process, and special attention in obtaining the inverse-DFT is required. Finite length structures, mainly short lengths, implies multiple reflections at smaller time scales and the response do not disappear within the chosen time window. This makes the response to wrap around, which means that part of the response beyond the chosen time window, will appear first. To avoid such distortion in the response a damped structure or a semi-infinite (throw-off) element needs to be be used with a large time window [25,3,26].

The treatment of uncertainties using spectral element method is recent [27,28], and very few was made related to detection and assessment of the damage. Recently, some researchers have presented works in damage detection using wave propagation in the context of uncertainty quantification and stochastic SEM model [29–32].

Structural health monitoring (SHM) can be defined as a process that involves the observation of a structure over time using periodically spaced measurements [33,34]. Based on this measurement the current state of the undamaged system can be determined. The inverse problem approach is a technique where the structural model parameters can be identified (or the damage can be detected) based on the frequency response data [35]. In general, the structural damage is a local phenomenon and produces a stiffness reduction, which changes the frequency response of the system [36]. Damage estimation is based on the optimisation methods [37,38], which can be used to solve the inverse problem. These techniques consist in minimising the differences between the numerical model and experimental test responses by using a parameter estimation procedure [39–41]. In structural dynamic testing, it is common practice to measure the data in the form of frequency response functions (FRF). The knowledge about a particular structure is contained in a theoretical model and can be constructed using a numerical method. Many papers written on this subject have been used with FEM [42] and the experimental modal analysis (EMA) [43]. In order to include parameter variability to damage detection and parameter estimation methods, recent researchers started with the stochastic approaches. Some authors [44,30,29] have proposed stochastic methods to characterise and identify the damage including random parameters based on probabilistic approaches. Arda Vanli and Sungmoon Jung [45], and Khodaparast and Mottershead [46] present a probabilistic and stochastic model updating method to improve damage location and damage quantification prediction of a structural health monitoring system.

Damage quantification methods assume that they can provide a numerical dynamic response very close to that of a real structure. Parameters, modelling, and measurement uncertainties are inherently involved in the damage quantification procedure. The stochastic approach in the framework to understand the magnitude of uncertainty for simulation results is evaluated. It can be treated in the scope of the random variable, which is understood as a function defined on a sample space whose outputs are numerical values, and random field corresponds to natural spatially varying properties [47]. The reference and most widely used method is the Monte Carlo (MC) simulation. It is a sampling method which can generate independent random variables, based on their probability distributions, and solving the deterministic problem for each realisation. By collecting an ensemble of solutions the statistical moments can be calculated [48]. Although easy to apply a large number of samples are needed to obtain convergence, which means high computational costs. The Direct method consists in directly applying the statistical moment equations to obtain the random solutions. The unknowns are the moments and their equations are derived by taking averages over the original stochastic governing equations. The problem is that a statistical moment almost always requires information about higher moments. A non-sampling approach, known as Perturbation method, consists of expanding the random fields in a truncated Taylor series around their mean. Its main drawback is the limitation of the magnitude of uncertainties which cannot be too large, typically less than 10% [49]. Another method widely used as considering random field is the Karhunen-Loève (KL) expansion [49,50]. The KL expansion may be used to discretize the random field by representing it by scalar independent random variables and continuous deterministic functions. By truncating the expansion the number of random variables becomes finite and numerically treatable. Several authors use the KL expansion to model Gaussian random processes, however it is possible to extend the KL expansion to non-Gaussian processes [51–58].

This work uses a rod structure modelled by SEM to localize and to assess a damage with parameter uncertainty related to material property and geometry. A rod structure was used to avoid the effects of evanescent waves at the first moment. The cross section area, density and Young's modulus were considered as a non-Gaussian random variable and as non-Gaussian distributed random field expanded by KL. A non-Gaussian process is expressed as a memoryless transformation of an underlying Gaussian process. The proposed stochastic damage quantification technique combines SEM with the stochastic approaches and Structural Health Monitoring procedure. Based on the mathematical structure model and the relation between undamaged and damaged structure an explicit formulation to estimate the damage localization and quantification was developed. This technique allows quantifying the damage by using directly the structural dynamic response and to improve the control over the numerical model dispersion when it is under a stochastic environment. One important advantage of the proposed spectral approach is that the analytical formulations are frequency band independent. Therefore, unlike conventional finite element based approaches, there is no limitation at high frequency ranges.

2. Spectral element method for stochastic systems

The spectral element method is similar to FEM with the exception of two important aspects. SEM is frequency domain formulation and the element interpolation function is the exact solution of wave equation. Based on this latter aspect the number of elements required for a spectral model will coincide with the number of structural discontinuities. In this section, it will be presented the stochastic formulation for undamaged and damaged rod spectral element. A damage localization and quantification technique

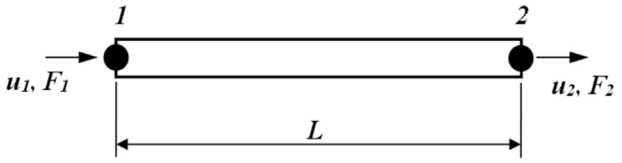

Fig. 1. Two nodes undamaged rod spectral element.

considering the stochastic process is presented. The new contribution consists in to obtain the structural response and crack parameters variability based on the uncertainty of structural parameter spatially distributed, using the random variable and random field approaches. The random field is expressed based on Karhunen-Loève expansion. A non-linear memoryless transformation is used to obtain a non-Gaussian random field from a Gaussian random field.

2.1. Undamaged rod

In this section, the fundamental equations are derived for a longitudinal wave propagation in an undamaged rod, a more extensive formulation can be found in [8,9]. The elementary rod theory considers this structure as long, slender, and assumes that it supports only 1-D axial stress. Fig. 1 shows an elastic two nodes rod element with one degree-of-freedom per node, uniform rectangular cross-section subjected to dynamic forces.

2.1.1. Deterministic

The undamped equilibrium equation with deterministic parameters at frequency domain can be written as [8]:

$$EA_0\frac{d^2u(x)}{dx^2} + \omega^2\rho A_0 u(x) = q(x), \tag{1}$$

where A is the cross-section area, ρ is the volume mass density, EA is the longitudinal rigidity, ρA is the mass per unit length, u is the longitudinal displacement, q is the distributed external force, and ω is the circular frequency. The subscript 0 indicates the mean values. A hysteretic structural damping is assumed and introduced into the model formulation by adding a complex damping factor in the Young's modulus. In the deterministic case it is a complex value given by $E = E_0(1 + i\eta)$, where E_0 is the Young's modulus mean value, η is the damping factor and $i = \sqrt{-1}$ [8]. In the stochastic case it is given by $E(\theta) = \widehat{E}(\theta) + E_0 i\eta$, where the random part of the Young's modulus is a real value, $\widehat{E}(\theta)$, and the deterministic part is the complex value $E_0 i\eta$.

The homogeneous solution of Eq. (1) is given by,

$$u(x) = a_1 e^{-ikx} + a_2 e^{-ik(L-x)} = \mathbf{s}(x, \omega)\mathbf{a}, \tag{2}$$

where a_i, $i = 1, 2$ are arbitrary constants, L is the rod element length, $k = \omega/c$ is the wavenumber corresponding to the longitudinal wave propagation, and $c = \sqrt{\rho A/EA}$ is the phase speed. In this case, the propagation is assumed to be non-dispersive as all frequency components travel at the same speed, so that the shape of the travelling wave remains the same, and

$$\mathbf{s}(x, \omega) = \{e^{-ikx}\ e^{-ik(L-x)}\}, \quad \mathbf{a} = \begin{Bmatrix} a_1 \\ a_2 \end{Bmatrix}. \tag{3}$$

The spectral nodal displacements of the rod can be related with the displacement field as,

$$\mathbf{d} = \begin{Bmatrix} u_1 \\ u_2 \end{Bmatrix} = \begin{Bmatrix} u(0) \\ u(L) \end{Bmatrix}. \tag{4}$$

By substituting Eq. (2) into the right side of Eq. (4) it has

$$\mathbf{d} = \begin{bmatrix} \mathbf{s}(0, \omega) \\ \mathbf{s}(L, \omega) \end{bmatrix}\mathbf{a} = \mathbf{G}(\omega)\mathbf{a}, \tag{5}$$

where

$$\mathbf{G}(\omega) = \begin{bmatrix} 1 & e^{-ikL} \\ e^{-ikL} & 1 \end{bmatrix}. \tag{6}$$

The frequency-dependent displacement within an element is interpolated from the nodal displacement vector $\mathbf{d}$. Substituting Eq. (5) in Eq. (2) the constant vector $\mathbf{a}$ is eliminated to obtain,

$$u(x, \omega) = \mathbf{g}(x, \omega)\mathbf{d}, \tag{7}$$

where the interpolation functions are given by,

$$\mathbf{g}(x, \omega) = \mathbf{s}(x, \omega)\mathbf{G}^{-1}(\omega) = \{g_1\ g_2\} \tag{8}$$

with $g_1 = \csc(kL)\sin[k(L - x)]$ and $g_2 = \csc(kL)\sin(kx)$. A generalized longitudinal displacement at any arbitrary point in the rod

element is given by $u(x) = g_1(x)u_1 + g_2(x)u_2$. By doing $\Gamma(\omega) = \mathbf{G}^{-1}(\omega)$ the mass and stiffness matrices are obtained as:

$$\mathbf{K}_0(\omega) = EA_0\ \mathbf{\Gamma}^T(\omega)\left[\int_0^L \mathbf{s}'^T(x,\omega)\mathbf{s}'(x,\omega)dx\right]\mathbf{\Gamma}(\omega), = \frac{EA_0k}{2}\begin{bmatrix}\csc^2(kL)(2kL+\sin(2kL))/2 & -(kL\cot(kL)+1)\csc(kL)\\ -(kL\cot(kL)+1)\csc(kL) & \csc^2(kL)(2kL+\sin(2kL))/2\end{bmatrix}. \tag{9}$$

$$\mathbf{M}_0(\omega) = \rho A_0\ \mathbf{\Gamma}^T(\omega)\left[\int_0^L \mathbf{s}^T(x,\omega)\mathbf{s}(x,\omega)dx\right]\mathbf{\Gamma}(\omega), = \frac{\rho A_0}{2k}\begin{bmatrix}(\cot(kL)-kL\csc^2(kL)) & (kL\cot(kL)-1)\csc(kL)\\ (kL\cot(kL)-1)\csc(kL) & (\cot(kL)-kL\csc^2(kL))\end{bmatrix}. \tag{10}$$

where $(\bullet)'$ is the first spacial derivative.

Then, the deterministic spectral undamaged rod element dynamic stiffness matrix is obtained as:

$$\mathbf{D}_0(\omega) = \mathbf{K}_0(\omega) - \omega^2\mathbf{M}_0(\omega). \tag{11}$$

2.1.2. Stochastic

The paper treats two different forms to consider uncertainty in the stochastic model. Most used approaches to treat data uncertainty are regard to random variables or random processes [49]. When the uncertainty is considered as random variables the Monte Carlo simulation can be used directly. If it is consider as a random process the Karhunen-Loève (KL) expansion decomposition needs to be applied. In this section the stochastic model for damaged and undamaged rods in axial vibration combining KL expansion and Spectral Element Method is presented.

Random field is discretized in terms of random variables. By doing this, many mathematical procedures can be used to solve the resulting discrete stochastic differential equations. The procedure applied here is a random field spectral decomposition using the KL expansion to localize and quantify structural damage. The random field is described by various points expressed by random variables, therefore, a large number of points is required for a good approximation. This concept is similar to the Fourier series expansion. Assuming that the covariance function is bounded, symmetric and positive definite, it can be represented by a spectral decomposition. By using this concept a random field can be expressed as a generalized Fourier series by,

$$\varpi(\mathbf{r},\theta) = \varpi_0(\mathbf{r}) + \sum_{j=1}^{\infty}\xi_j(\theta)\sqrt{\lambda_j}\varphi_j(\mathbf{r}), \tag{12}$$

where $\varpi(\mathbf{r},\theta)$ is a random field with the covariance function $C_{\varpi}(\mathbf{r}_1,\mathbf{r}_2)$ defined in a space $\mathcal{D}$. Here θ denotes an element of the sample space Ω, so that $\theta \in \Omega$; $\xi_j(\theta)$ are uncorrelated random variables. The subscript 0, $\varpi_0(\mathbf{r})$, implies the corresponding deterministic part. The constants λ_j and functions $\varphi_j(\mathbf{r})$ are, respectively, eigenvalues and eigenfunctions satisfying the the Fredholm integral equation,

$$\int_{\mathcal{D}} C_{\varpi}(\mathbf{r}_1,\mathbf{r}_2)\varphi_j(\mathbf{r}_1)d\mathbf{r}_1 = \lambda_j\varphi_j(\mathbf{r}_2) \quad \forall\, j = 1, 2, \ldots. \tag{13}$$

The spectral decomposition of covariance function implies the solution of equation (13). For some covariance functions it can be solved analytically, such as the first-order Markov processes given by,

$$C(x_1, x_2) = e^{-|x_1-x_2|/\mathrm{b}}, \tag{14}$$

where $\mathrm{b} > 0$ is the correlation length, which is an important parameter to describe the random field. A random field becomes a random variable if the correlation length is large as compared with the domain under consideration. A brief explanation for the analytical solution defining the process in the interval $[-\mathrm{a} < x < \mathrm{a}]$ is presented in the following, a more detailed development can be found in the book of Ghanem and Spanos [50].

Substituting Eq. (14) into Eq. (13) produces,

$$\int_{-\mathrm{a}}^{\mathrm{a}} e^{-\mathrm{c}|x_1-x_2|}\varphi(x_1)dx_1 = \lambda\varphi(x_2), \tag{15}$$

where $\mathrm{c} = 1/\mathrm{b}$. Eq. (15) can be rewritten as,

$$\int_{-\mathrm{a}}^{x_1} e^{-\mathrm{c}(x_1-x_2)}\varphi(x_1)dx_1 + \int_{x_1}^{\mathrm{a}} e^{-\mathrm{c}(x_2-x_1)}\varphi(x_1)dx_1 = \lambda\varphi(x_2). \tag{16}$$

Differentiating Eq. (16) twice with respect to x_1 gives

$$\lambda\varphi''(x) = (-2\mathrm{c} + \mathrm{c}^2\lambda)\varphi(x). \tag{17}$$

Defining the variable $w^2 = (2\mathrm{c} - \mathrm{c}^2\lambda)/\lambda$, Eq. (17) becomes,

$$\varphi''(x) + w^2\varphi(x) = 0. \tag{18}$$

By solving simultaneously the Eq. (18) together with the equations of associated boundary conditions, the eigenvalues and eigenfunctions for odd j are given by

$$\lambda_j = \frac{2c}{w_j^2 + c^2}; \quad \varphi_j(x) = \frac{\cos(w_j x)}{\sqrt{a + \dfrac{\sin(2w_j a)}{2w_j}}} \quad \text{where } \tan(w_j a) = \frac{c}{w_j}, \tag{19}$$

and for even j are given by

$$\lambda_j = \frac{2c}{w_j^2 + c^2}; \quad \varphi_j(x) = \frac{\sin(w_j x)}{\sqrt{a - \dfrac{\sin(2w_j a)}{2w_j}}} \quad \text{where } \tan(w_j a) = \frac{w_j}{-c} \tag{20}$$

for $x = L/2$. These eigenvalues and eigenfunctions will be used to obtain the stochastic dynamic stiffness matrices for undamaged and damaged rod spectral elements.

For practical applications, the Eq. (12) is truncated with N numbers of terms, which could be selected based on the amount of information to be kept. Its value is also related to the correlation length and the number of eigenvalues kept, provided that they are arranged in decreasing order [27].

In KL assumption, the processes is an underlying Gaussian. However, it is not applicable for most of the physical systems which, on the contrary, are expected to be characterised by non-linear behaviours [53]. In this paper it will be consider the numerical simulation of non-Gaussian process. Based on the assumption of the KL expansion a non-Gaussian process is expressed as a memoryless transformation of an underlying Gaussian process. The covariance function $C(x_1, x_2)$ of the underlying Gaussian process is chosen so that the transformation leads to a non-Gaussian process with the proposed covariance function $C_s(x_1, x_2)$. A non-Gaussian process $\varpi(x, \theta)$ is expressed as a memoryless transformation of an underlying standard Gaussian process $Z(\mathbf{x}, \theta)$ by means of the cumulative density functions (CDF) of both processes:

$$\varpi(\mathbf{x}, \theta) = F_{\varpi x}^{-1}(F_Z(Z(\mathbf{x}, \theta))), \tag{21}$$

where $F_{\varpi x}(\varpi)$ is the marginal CDF of the non-Gaussian process and $F_Z(z)$ is the standard Gaussian CDF. An approximation of the transformation can be obtained in terms of the one-dimensional Hermite polynomials of order P:

$$\varpi(\mathbf{x}, \theta) \approx \sum_{n=0}^{P} a_n(\mathbf{x}) h_n(Z(\mathbf{x}, \theta)). \tag{22}$$

The coefficients $\{a_n(x)\}_n$ are obtained based on orthonormality of the Hermite polynomials $\{h_n(z)\}_n$ [59,60] and a stationary process, which can be expressed as:

$$a_n(\mathbf{x}) = \int_{\infty}^{\infty} F_{Yx}^{-1}(F_Z(z)) h_n(z) p_Z(z) dz. \tag{23}$$

Equating the covariance of Eq. (21) leads to

$$C_s(\mathbf{x}_1, \mathbf{x}_2) \approx \sum_{n=0}^{P} a_n(\mathbf{x}_1) a_n(\mathbf{x}_2) [C(\mathbf{x}_1, \mathbf{x}_2)]^n. \tag{24}$$

If $\varpi(\mathbf{x}, \theta)$ is a stationary process, then the covariance reduces to

$$C_s(\Delta\mathbf{x}) \approx \sum_{n=0}^{P} a_n^2 [C(\Delta\mathbf{x})]^n. \tag{25}$$

The same undamaged rod analytical model considered in the deterministic formulation is used here for the stochastic formulation. Now it is assumed that cross-section area, mass density, and Young's modulus are random variables spatially distributed. Therefore, the longitudinal rigidity (EA) and mass per unit length (ρA) are assumed, respectively, as random field of the form

$$EA(x, \theta) = EA_0[1 + \varepsilon_1 \varpi_1(x, \theta)]; \quad \rho A(x, \theta) = \rho A_0[1 + \varepsilon_2 \varpi_2(x, \theta)], \tag{26}$$

where the subscript 0 indicates the underlying baseline model and ε_i are deterministic constants ($0 < \varepsilon_i \ll 1$, $i = 1, 2$). The random fields $\varpi_i(x, \theta)$, $i = 1, 2$ are taken to have zero mean, unit standard deviation and covariance $C_{ij}(\xi)$. Since, $EA(x, \theta)$ and $\rho A(x, \theta)$ are strictly positive, $\varpi_i(x, \theta)$ are required to satisfy the probability condition $P[1 + \varepsilon_i \varpi_i(x, \theta) \le 0] = 0$. To obtain the stiffness and mass matrices associated with the random components, for each j, two different matrices correspond to the two eigenfunctions defined in Eqs. (19) and (20) as

$$\mathbf{K}(\omega, \theta) = \mathbf{K}_0(\omega) + \Delta\mathbf{K}(\omega, \theta); \quad \mathbf{M}(\omega, \theta) = \mathbf{M}_0(\omega) + \Delta\mathbf{M}(\omega, \theta), \tag{27}$$

where $\Delta\mathbf{K}_e(\omega, \theta)$ and $\Delta\mathbf{M}_e(\omega, \theta)$ are the random part of the stiffness and mass matrices. From the KL expansion and Eqs. (26), this matrices can be conveniently expressed as,

$$\Delta\mathbf{K}(\omega, \theta) = \varepsilon_1 \sum_{j=1}^{N} \xi_{Kj}(\theta) \sqrt{\lambda_{Kj}} \mathbf{K}_j(\omega); \quad \Delta\mathbf{M}(\omega, \theta) = \varepsilon_2 \sum_{j=1}^{N} \xi_{Mj}(\theta) \sqrt{\lambda_{Mj}} \mathbf{M}_j(\omega), \tag{28}$$

where N is the number of terms kept in the KL expansion, $\xi_{Kj}(\theta)$ and $\xi_{Mj}(\theta)$ are uncorrelated Gaussian random variables with zero mean

and unit standard deviation. The matrices $\mathbf{K}_j(\omega)$ and $\mathbf{M}_j(\omega)$ are written as

$$\mathbf{K}_j(\omega) = EA_0\boldsymbol{\Gamma}^T(\omega)\left[\int_0^L \varphi_{Kj}(x_e + x)\mathbf{s}'(x,\omega)^T\mathbf{s}'(x,\omega)dx\right]\boldsymbol{\Gamma}(\omega), \tag{29}$$

$$\mathbf{M}_j(\omega) = \rho A_0\boldsymbol{\Gamma}^T(\omega)\left[\int_0^L \varphi_{Mj}(x_e + x)\mathbf{s}(x,\omega)^T\mathbf{s}(x,\omega)dx\right]\boldsymbol{\Gamma}(\omega). \tag{30}$$

Substituting Eqs. (19) and (20) in Eqs. (29) and (30) the random part of the stiffness and mass element matrices in a closed-form expressions with odd j are, respectively, given by

$$\mathbf{K}_j^{odd}(\omega) = \frac{EA_0}{\sqrt{\mathrm{a} + \dfrac{\sin(2w_j\mathrm{a})}{2w_j}}}\boldsymbol{\Gamma}^T(\omega)\left[\int_0^L \cos(\omega_j(x_e + x))\mathbf{s}'(x,\omega)^T\mathbf{s}'(x,\omega)dx\right]\boldsymbol{\Gamma}(\omega) = \frac{EA_0}{\sqrt{\mathrm{a} + \dfrac{\sin(2w_j\mathrm{a})}{2w_j}}}\begin{bmatrix} Ko_{11} & Ko_{12} \\ Sym & Ko_{22}\end{bmatrix}; \tag{31}$$

$$\mathbf{M}_j^{odd}(\omega) = \frac{\rho A_0}{\sqrt{\mathrm{a} + \dfrac{\sin(2w_j\mathrm{a})}{2w_j}}}\boldsymbol{\Gamma}^T(\omega)\left[\int_0^L \cos(\omega_j(x_e + x))\mathbf{s}(x,\omega)^T\mathbf{s}(x,\omega)dx\right]\boldsymbol{\Gamma}(\omega) = \frac{\rho A_0}{\sqrt{\mathrm{a} + \dfrac{\sin(2w_j\mathrm{a})}{2w_j}}}\begin{bmatrix} Mo_{11} & Mo_{12} \\ Sym & Mo_{22}\end{bmatrix}, \tag{32}$$

and for even j are, respectively, given by

$$\mathbf{K}_j^{even}(\omega) = \frac{EA_0}{\sqrt{\mathrm{a} - \dfrac{\sin(2w_j\mathrm{a})}{2w_j}}}\boldsymbol{\Gamma}^T(\omega)\left[\int_0^L \sin(\omega_j(x_e + x))\mathbf{s}'(x,\omega)^T\mathbf{s}'(x,\omega)dx\right]\boldsymbol{\Gamma}(\omega) = \frac{EA_0}{\sqrt{\mathrm{a} - \dfrac{\sin(2w_j\mathrm{a})}{2w_j}}}\begin{bmatrix} Ke_{11} & Ke_{12} \\ Sym & Ke_{22}\end{bmatrix}; \tag{33}$$

$$\mathbf{M}_j^{even}(\omega) = \frac{\rho A_0}{\sqrt{\mathrm{a} - \dfrac{\sin(2w_j\mathrm{a})}{2w_j}}}\boldsymbol{\Gamma}^T(\omega)\left[\int_0^L \sin(\omega_j(x_e + x))\mathbf{s}(x,\omega)^T\mathbf{s}(x,\omega)dx\right]\boldsymbol{\Gamma}(\omega) = \frac{\rho A_0}{\sqrt{\mathrm{a} - \dfrac{\sin(2w_j\mathrm{a})}{2w_j}}}\begin{bmatrix} Me_{11} & Me_{12} \\ Sym & Me_{22}\end{bmatrix}. \tag{34}$$

The exact closed-form expression of the elements, Ko_{ij}, Mo_{ij}, Ke_{ij}, Me_{ij}, of these four matrices (Eqs. (31)–(34)) are given in Appendix A.

Substituting Eqs. (31)–(34) into the Eqs. (27) the stochastic spectral undamaged rod element stiffness and mass matrices, $\mathbf{K}(\omega, \theta)$ and $\mathbf{M}(\omega, \theta)$, can be obtained. Then, the stochastic spectral undamaged rod element dynamic stiffness matrix is obtained as:

$$\mathbf{D}(\omega, \theta) = \mathbf{K}(\omega, \theta) - \omega^2\mathbf{M}(\omega, \theta). \tag{35}$$

2.2. Damaged rod

This section presents the formulation for a spectral rod element with a transverse, open and non-propagating crack [3,61]. Fig. 2 shows a two-nodes rod element with uniform rectangular cross-section, length L, crack position L_1, and crack depth a. The crack is modelled as a dimensionless and local flexibility, Θ, which is calculated by Castigliano's theorem and the laws of fracture mechanics [62].

2.2.1. Deterministic

The homogeneous displacement solution for Eq. (1) applied for this element must be described in two parts, one for the left-hand side of the crack and other for the right-hand side of the crack, then

$$u_L(x) = a_1e^{-ikx} + a_2e^{-ik(L_1-x)} \quad (0 \le x \le L_1) = \mathbf{s}_L(x;\omega)\mathbf{a}_L, \tag{36}$$

where $\mathbf{s}_L(x,\omega) = [e^{-ikx}\ e^{-ik(L_1-x)}]$; and $\mathbf{a}_L = \{a_1\ a_2\}^T$;

$$u_R(x) = a_3e^{-ik(x+L_1)} + a_4e^{-ik[L-(L_1+x)]} \quad (0 \le x \le L - L_1) = \mathbf{s}_R(x;\omega)\mathbf{a}_R, \tag{37}$$

where $\mathbf{s}_R(x,\omega) = [e^{-ik(x+L_1)}\ e^{-ik[L-(L_1+x)]}$; and $\mathbf{a}_R = \{a_3\ a_4\}^T$. Writing the Eq. (36) and (37) in matrix form it has,

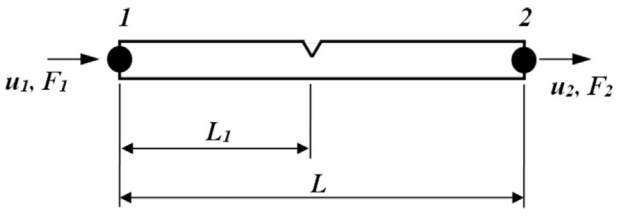

Fig. 2. Two-node damaged rod spectral element.

$$\begin{Bmatrix} u_L(x) \\ u_R(x) \end{Bmatrix} = \begin{bmatrix} \mathbf{s}_L(x,\,\omega) & \mathbf{0} \\ \mathbf{0} & \mathbf{s}_R(x,\,\omega) \end{bmatrix} \begin{Bmatrix} \mathbf{a}_L \\ \mathbf{a}_R \end{Bmatrix} = \mathbf{s}_d(x,\,\omega)\mathbf{a}_d. \tag{38}$$

The coefficients vector $\mathbf{a}_d$ can be calculated as a function of the nodal spectral displacements using the element boundary and compatibility conditions at the element left-end $u_L(0) = u_1$; at the element cracked cross-section $u_L(L_1) - u_R(0) = \Theta\partial u/\partial x$; at the element non-cracked cross-section $\partial u_L(L_1)/\partial x = \partial u_R(0)/\partial x$; and at the element right-end $u_R(L - L_1) = u_2$. Coupling the damaged element left and right-hand sides (Eqs. (36) and (37)) and applying boundary and compatibility conditions it has,

$$\underbrace{\begin{bmatrix} 1 & e^{-ikL_1} & 0 & 0 \\ (ik\Theta - 1)e^{-ikL_1} & (ik\Theta - 1) & e^{-ikL_1} & e^{-ik(L-L_1)} \\ -ike^{-ikL_1} & ik & ike^{-ikL_1} & -ike^{-ik(L-L_1)} \\ 0 & 0 & e^{-ikL} & 1 \end{bmatrix}}_{\mathbf{G}_d} \begin{Bmatrix} a_1 \\ a_2 \\ a_3 \\ a_4 \end{Bmatrix} = \begin{Bmatrix} u_1 \\ 0 \\ 0 \\ u_2 \end{Bmatrix}. \tag{39}$$

Eq. (39) can be rewritten in a compact for as

$$\mathbf{a}_d = \mathbf{G}_{dr}^{-1}\mathbf{d}_d, \tag{40}$$

where $\mathbf{d}_d = \{u_1\ u_2\}^T$ is the element node displacement vector without zeros, and $\mathbf{G}_{dr}^{-1}$ is the inverse of $\mathbf{G}_d$ in corresponding reduced dimension, given by

$$\mathbf{G}_d^{-1} = \begin{bmatrix} \frac{e^{ikL_1}((k\Theta - i)\cos(k(L-L_1)) + \sin(k(L-L_1)))}{k\Theta(\cos(kL) + \cos(k(L-2L_1))) + 2\sin(kL)} & \frac{i}{k\Theta(\cos(kL) + \cos(k(L-2L_1))) + 2\sin(kL)} \\ \frac{(k\Theta + i)\cos(k(L-L_1)) + \sin(k(L-L_1))}{k\Theta(\cos(kL) + \cos(k(L-2L_1))) + 2\sin(kL)} & -\frac{ie^{ikL_1}}{k\Theta(\cos(kL) + \cos(k(L-2L_1))) + 2\sin(kL)} \\ -\frac{ie^{ikL}}{k\Theta(\cos(kL) + \cos(k(L-2L_1))) + 2\sin(kL)} & \frac{(1 + e^{2ikL_1})k\Theta + 2i}{2k\Theta(\cos(kL) + \cos(k(L-2L_1))) + 4\sin(kL)} \\ \frac{i}{k\Theta(\cos(kL) + \cos(k(L-2L_1))) + 2\sin(kL)} & \frac{e^{ik(L-L_1)}((k\Theta - i)\cos(kL_1) + \sin(kL_1))}{k\Theta(\cos(kL) + \cos(k(L-2L_1))) + 2\sin(kL)} \end{bmatrix}. \tag{41}$$

Substituting Eq. (40) in (38) it has,

$$\begin{Bmatrix} u_L(x) \\ u_R(x) \end{Bmatrix} = \begin{bmatrix} \mathbf{s}_L(x,\,\omega) & \mathbf{0} \\ \mathbf{0} & \mathbf{s}_R(x,\,\omega) \end{bmatrix} \mathbf{G}_{dr}^{-1}\mathbf{d}_d = \mathbf{g}_d(x,\,\omega)\mathbf{d}_d \tag{42}$$

where $\mathbf{g}_d(x,\,\omega) = \mathbf{s}_d\mathbf{G}_{dr}^{-1}$.

For the damaged rod model, the stiffness matrix must be integrated according to the corresponding limits for left-hand and right-hand sides of crack position. By doing $\mathbf{\Gamma}_d(\omega) = \mathbf{G}_{dr}^{-1}$ the deterministic stiffness element matrix is obtained as:

$$\mathbf{K}_{0_d}(\omega) = EA_0\ \mathbf{\Gamma}_d^T(\omega) \begin{bmatrix} \int_0^{L_1} \mathbf{s}_{L'}^T(x,\,\omega)\mathbf{s}'_L(x,\,\omega)dx & \mathbf{0} \\ \mathbf{0} & \int_0^{(L-L_1)} \mathbf{s}_{R'}^T(x,\,\omega)\mathbf{s}'_R(x,\,\omega)dx \end{bmatrix} \mathbf{\Gamma}_d(\omega), = \begin{bmatrix} K_{0d_{11}} & K_{0d_{12}} \\ sym & K_{0d_{22}} \end{bmatrix}. \tag{43}$$

Similarly, the damage rod deterministic mass element matrix is obtained as:

$$\mathbf{M}_{0_d}(\omega) = \rho A_0\ \mathbf{\Gamma}_d^T(\omega) \begin{bmatrix} \int_0^{L_1} \mathbf{s}_L^T(x,\,\omega)\mathbf{s}_L(x,\,\omega)dx & \mathbf{0} \\ \mathbf{0} & \int_0^{(L-L_1)} \mathbf{s}_R^T(x,\,\omega)\mathbf{s}_R(x,\,\omega)dx \end{bmatrix} \mathbf{\Gamma}_d(\omega), = \begin{bmatrix} M_{0d_{11}} & M_{0d_{12}} \\ sym & M_{0d_{22}}. \end{bmatrix}. \tag{44}$$

The exact closed-form expression of the elements, $K_{0d_{ij}}$ and $M_{0d_{ij}}$ i and j=1,2, of these two matrices (Eqs. (43) and (44)) are given in Appendix B.1.

The deterministic spectral damaged rod element dynamic stiffness matrix is obtained as:

$$\mathbf{D}_{0_d}(\omega) = \mathbf{K}_{0_d}(\omega) - \omega^2\mathbf{M}_{0_d}(\omega). \tag{45}$$

2.2.2. Stochastic

Likewise the stochastic undamaged rod formulation, the stochastic dynamic stiffness element matrix for the damaged rod spectral element, $\mathbf{D}_d(\omega,\,\theta)$, is developed. The same damaged rod analytical model considered in the deterministic formulation is used here for the stochastic formulation. However, it is assumed that A, E, ρ are now random variables, and EA and ρA are random fields. We can express the stochastic damaged rod stiffness and mass element matrices, respectively, as:

$$\mathbf{K}_d(\omega,\,\theta) = \mathbf{K}_{0_d}(\omega) + \Delta\mathbf{K}_d(\omega,\,\theta); \quad \mathbf{M}_d(\omega,\,\theta) = \mathbf{M}_{0_d}(\omega) + \Delta\mathbf{M}_d(\omega,\,\theta) \tag{46}$$

From the KL expansion and Eqs. (26) it has,

$$\Delta\mathbf{K}_d(\omega,\theta)=\varepsilon_1\sum_{j=1}^{N}\xi_{Kj}(\theta)\sqrt{\lambda_{Kj}}\mathbf{K}_{j_d}(\omega); \tag{47}$$

$$\Delta\mathbf{M}_d(\omega,\theta)=\varepsilon_2\sum_{j=1}^{N}\xi_{Mj}(\theta)\sqrt{\lambda_{Mj}}\mathbf{M}_{j_d}(\omega) \tag{48}$$

where N is the number of terms kept in the KL expansion, $\xi_{Kj}(\theta)$ and $\xi_{Mj}(\theta)$ are uncorrelated Gaussian random variables with zero mean and unit standard deviation. By considering different limits of integration (left- and right-hand sides) for the damaged rod model it has,

$$\mathbf{K}_{j_d}(\omega)=EA_0\boldsymbol{\Gamma}_d^T(\omega)\begin{bmatrix}\mathbf{Sk}_L & \mathbf{0}\\ \mathbf{0} & \mathbf{Sk}_R\end{bmatrix}\boldsymbol{\Gamma}_d(\omega), \tag{49}$$

$$\mathbf{M}_{j_d}(\omega)=\rho A_0\boldsymbol{\Gamma}_d^T(\omega)\begin{bmatrix}\mathbf{Sm}_L & \mathbf{0}\\ \mathbf{0} & \mathbf{Sm}_R\end{bmatrix}\boldsymbol{\Gamma}_d(\omega), \tag{50}$$

where

$$\mathbf{Sk}_L=\int_0^{L_1}\varphi_{Kj}(x_e+x)\mathbf{s}_L^T(x,\omega)\mathbf{s'}_L(x,\omega)dx\mathbf{Sk}_R=\int_0^{(L-L_1)}\varphi_{Kj}(x_e+x)\mathbf{s}_R^T(x,\omega)\mathbf{s'}_R(x,\omega)dx\mathbf{Sm}_L=\int_0^{L_1}\varphi_{Mj}(x_e+x)\mathbf{s}_L^T(x,\omega)\mathbf{s}_L(x,\omega)$$
$$dx\mathbf{Sm}_R=\int_0^{(L-L_1)}\varphi_{Mj}(x_e+x)\mathbf{s}_R^T(x,\omega)\mathbf{s}_R(x,\omega)dx \tag{51}$$

Substituting Eqs. (19) and (20) in Eqs. (49) and (50) the random part of the stiffness and mass matrices as closed-form expressions can be obtained. However, these are huge closed-form expressions not easily workable. Then, Eqs. (49) and (50) were solved with MATHEMATICA® software and exported directly to the MATLAB® code to obtain the numerical solutions. As a matter of understanding and reproducibility of results it is shown here only the matrices form of $\mathbf{Sk}_L$, $\mathbf{Sk}_R$, $\mathbf{Sm}_L$, $\mathbf{Sm}_R$ for odd and even j^{th} terms. By considering odd j it has,

$$\mathbf{Sk}_L^{odd}(\omega)=\frac{EA_0}{\sqrt{\mathrm{a}+\frac{\sin(2w_j\mathrm{a})}{2w_j}}}\begin{bmatrix}SkLo_{11} & SkLo_{12}\\ Sym & SkLo_{22}\end{bmatrix}\mathbf{Sk}_R^{odd}(\omega)=\frac{EA_0}{\sqrt{\mathrm{a}+\frac{\sin(2w_j\mathrm{a})}{2w_j}}}\begin{bmatrix}SkRo_{11} & SkRo_{12}\\ Sym & SkRo_{22}\end{bmatrix}\mathbf{Sm}_L^{odd}(\omega)$$
$$=\frac{\rho A_0}{\sqrt{\mathrm{a}+\frac{\sin(2w_j\mathrm{a})}{2w_j}}}\begin{bmatrix}SmLo_{11} & SmLo_{12}\\ Sym & SmLo_{22}\end{bmatrix}\mathbf{Sm}_R^{odd}(\omega)=\frac{\rho A_0}{\sqrt{\mathrm{a}+\frac{\sin(2w_j\mathrm{a})}{2w_j}}}\begin{bmatrix}SmRo_{11} & SmRo_{12}\\ Sym & SmRo_{22}\end{bmatrix} \tag{52}$$

and for even j it has,

$$\mathbf{Sk}_L^{even}(\omega)=\frac{EA_0}{\sqrt{\mathrm{a}-\frac{\sin(2w_j\mathrm{a})}{2w_j}}}\begin{bmatrix}SkLe_{11} & SkLe_{12}\\ Sym & SkLe_{22}\end{bmatrix}\mathbf{Sk}_R^{even}(\omega)=\frac{EA_0}{\sqrt{\mathrm{a}-\frac{\sin(2w_j\mathrm{a})}{2w_j}}}\begin{bmatrix}SkRe_{11} & SkRe_{12}\\ Sym & SkRe_{22}\end{bmatrix}\mathbf{Sm}_L^{even}(\omega)$$
$$=\frac{\rho A_0}{\sqrt{\mathrm{a}-\frac{\sin(2w_j\mathrm{a})}{2w_j}}}\begin{bmatrix}SmLe_{11} & SmLe_{12}\\ Sym & SmLe_{22}\end{bmatrix}\mathbf{Sm}_R^{even}(\omega)=\frac{\rho A_0}{\sqrt{\mathrm{a}-\frac{\sin(2w_j\mathrm{a})}{2w_j}}}\begin{bmatrix}SmRe_{11} & SmRe_{12}\\ Sym & SmRe_{22}\end{bmatrix} \tag{53}$$

The exact closed-form expression of each element, $\{SkLo_{ij}, SmLo_{ij}, SkRo_{ij}, SmRo_{ij}\}$ and $\{SkLe_{ij}, SmLe_{ij}, SkRe_{ij}, SmRe_{ij}\}$, of these eight matrices are given in Appendix B.2.

The stochastic spectral damaged rod element dynamic stiffness matrix is obtained as:

$$\mathbf{D}_d(\omega,\theta)=\mathbf{K}_d(\omega,\theta)-\omega^2\mathbf{M}_d(\omega,\theta). \tag{54}$$

2.2.3. Crack flexibility

The crack flexibility coefficient (Θ) is calculated using Castigliano's theorem, where the flexibility at crack position for the one-dimensional rod spectral element is obtained as in reference [25]. Fig. 3 shows the damaged rod element cross-section at the crack position, including the new dimensionless crack depth defined as $\alpha=a/h$.

Crack flexibility coefficient can be written as a function of crack depth as,

$$\mathrm{c}(\alpha)=\frac{2\pi}{Eb}\int_0^{\alpha}\alpha\mathrm{f}(\alpha)^2d\alpha,$$

where f is a correction function of the form [62]:,

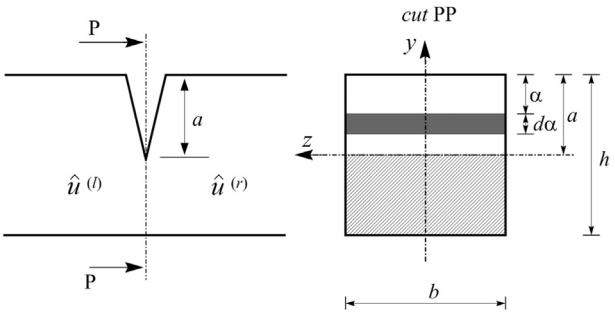

Fig. 3. Damaged rod cross-section at the crack position.

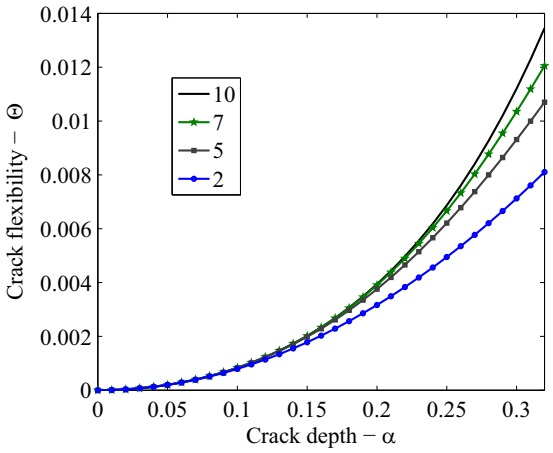

Fig. 4. Crack flexibility coefficient versus crack depth using polynomial equation of degree 2, 5, 7 and 10.

$$f(\alpha) = 1.122 - 0.231\alpha + 10.550\alpha^2 - 21.710\alpha^3 + 30.382\alpha^4.$$

It can be shown that the dimensionless local crack flexibility can be written as [25]:

$$\Theta = 2\pi h \int_0^{\alpha} \alpha f(\alpha)^2 d\alpha. \tag{55}$$

3. Explicit crack detection

By solving the integral in Eq. (55), the crack flexibility coefficient (Θ) is obtained as:

$$\Theta(\alpha) = 2\pi h(0.63\alpha^2 - 0.17\alpha^3 + 5.93\alpha^4 - 10.72\alpha^5 + 31.58\alpha^6 - 67.44\alpha^7 + 139.05\alpha^8 - 146.58\alpha^9 + 92.30\alpha^{10}). \tag{56}$$

Since the rod crack depth is a variable that physically quantifies the damage, it is important to find out an explicit equation to obtain it. Nevertheless, the dynamic spectral matrix for the damaged rod element (Eq. (41)) is a function of Θ, which is a polynomial equation of degree 10 in α. To obtain a simple and feasible explicit solution for α, the crack flexibility polynomial equation is approximated by its first term (degree 2). To verify the limits for this approximation crack flexibility coefficient (Eq. (56)) is calculated with degrees $n = \{2, 5, 7, 10\}$. Fig. 4 shows the results where for a crack depth value up to 0.13, crack flexibility does not change significantly for all degrees. To crack depth values higher than that, the divergence among curves increase as the degree of polynomial increases.

In structural dynamic testing, it is a common practice to measure the data in the form of frequency response function (FRF). The knowledge about a particular structure will be contained in an analytical (or numerical) model. The theoretical FRF obtained from the analytical model here is the inverse of the dynamic stiffness matrix for structural systems. Many damage quantification methods use of comparing the undamaged with the damaged response of the system. One of them, called Damage Index (DI) define the average power reduction between the damaged and undamaged state signals [6]. Others authors [63,64,34,65] proposed the percentage changes in the natural frequencies between the system undamaged and damaged states. Regarding this principle, we used a damage indicator defined as *relative change* between the damaged and undamaged FRF's system given by:

$$\mathbf{\Lambda}(\omega) = \frac{\mathbf{H}_d(\omega) - \mathbf{H}_u(\omega)}{\mathbf{H}_u(\omega)}, \tag{57}$$

where $\mathbf{H}_d(\omega) = [\mathbf{D}_{0_d}(\omega)]^{-1}$ is the damaged rod FRF, $\mathbf{H}_u(\omega) = [\mathbf{D}_0(\omega)]^{-1}$ is the undamaged rod FRF, and ω is the circular frequency. Rod FRF matrix can be written as,

$$\mathbf{H} = \begin{bmatrix} \mathbf{H}^{(11)} & \mathbf{H}^{(12)} \\ \mathbf{H}^{(21)} & \mathbf{H}^{(22)} \end{bmatrix}, \tag{58}$$

where $\mathbf{H}^{(ij)}$ is a FRF with response at element node i and excitation at element node j. To formulate explicit equations for crack depth and position, it is consider a transfer receptance FRF, e.g $\mathbf{H}^{(21)}$, for damaged and undamaged rod models. The analytical and measured FRF are used to calculate relative change, respectively, as

$$\mathbf{\Lambda}_{an}(\omega) = \frac{\mathbf{H}_{d_{an}}^{(21)} - \mathbf{H}_{u_{an}}^{(21)}}{\mathbf{H}_{u_{an}}^{(21)}}; \quad \mathbf{\Lambda}_m(\omega) = \frac{\mathbf{H}_{d_m}^{(21)} - \mathbf{H}_{u_m}^{(21)}}{\mathbf{H}_{u_m}^{(21)}}, \tag{59}$$

where measured FRF is the effect data which can be obtained experimentally (or numerically simulated), and the analytical FRF means the symbolic mathematical expression. The relative change using analytical FRF for a rod with two nodes is given by,

$$\mathbf{\Lambda}_{an}(\omega) = \frac{\Theta k(-2\sin^2(k(L-L_1)) - \cos(kL) + \cos(k(L-2L_1)))}{(\cos(kL))(\Theta k(\cos(kL) - \cos(k(L-2L_1))) - 2\sin(kL))}. \tag{60}$$

Similarly to the model updating approach, the inverse problem will be applied here as a technique where the structural damage parameters (α and L_1) will be estimated based on the minimization of the difference between analytical and measured FRF relative change [39,40,1] expressed by,

$$\mathbf{\Lambda}_{an}(\omega) - \mathbf{\Lambda}_m(\omega) = \varepsilon_{\mathbf{\Lambda}}. \tag{61}$$

Substituting Eq. (60) into (61) and assuming that modelling and measurements errors are negligible ($\varepsilon_\Lambda = 0$) it has,

$$\frac{\Theta k(-2\sin^2(k(L-L_1)) - \cos(kL) + \cos(k(L-2L_1)))}{(\cos(kL))(\Theta k(\cos(kL) - \cos(k(L-2L_1))) - 2\sin(kL))} - \mathbf{\Lambda}_m(\omega) = 0. \tag{62}$$

Approximating crack flexibility coefficient by its first term, $\Theta = 2\pi h(0.63\alpha^2)$, substituting in Eq. (62), solving in MATHEMATICA® software and simplifying, an explicit expression for crack depth is obtained as,

$$\boldsymbol{\alpha}(\omega) = \left| \frac{0.711[\mathbf{\Lambda}_m \sin(kL)]^{1/2}}{\{hk[\mathbf{\Lambda}_m(\cos(kL) - \cos(k(L-2L_1))) + \cos(kL) - \cos(k(L-2L_1))]\}^{1/2}} \right|. \tag{63}$$

Using the same approximation for Θ and expanding trigonometric functions in Eq. (62) with the first two non-zero terms of power series, solving in MATHEMATICA® software and simplifying, an explicit expression for the crack position is obtained as,

$$L_1(\omega) = \left| \frac{0.7071i}{k} \left\{ \cos(kL) - 1 - \left[\frac{0.5052\mathbf{\Lambda}_m \sin(kL)}{hk\alpha^2(\mathbf{\Lambda}_m + 1)} \right] \right\}^{1/2} \pm \left(\frac{L}{2} \right) \right|. \tag{64}$$

The relative percent error between nominal (a given value) and the approximated (first term of Eq. (56)) crack depth, and the relative percent error between nominal (a given value) and approximated (two first terms of power series) crack position are expressed as,

$$\varepsilon_\alpha = \left| \frac{\alpha_{no}(\omega) - \alpha(\omega)}{\alpha_{no}(\omega)} \right| \times 100; \quad \varepsilon_{L_1} = \left| \frac{L_1^{no}(\omega) - L_1(\omega)}{L_1^{no}(\omega)} \right| \times 100,$$

where α_{no} is a given nominal crack depth at a given nominal crack position L_1^{no}. These nominal values are used to obtain the measured FRF relative change (Λ_m) using the complete equation of crack flexibility (Eq. (56)) and the Eq. (62). Then, Λ_m is substituted into Eqs. (63) and (64) to obtain the calculated crack depth (α) and crack position L_1, respectively. Substituting α_{no}, α, L_1^{no}, and L_1 into the Eq. (65) the crack depth and position percent error are obtained.

3.1. Average measured FRF relative change

In the procedure to estimate the crack depth (Eq. (63)) and crack position (Eq. (64)) presented in the Section 3, it will be required to obtain a measured FRF relative change. In this paper, the stochastic rod models will be used to calculate the measured FRF to obtain $\Lambda_m(\omega, \theta)$. Three statistical approaches are used:

- Mathematical expectation of the measured FRF relative change, which can be expressed as,

$$\mathbf{\Lambda}_m^{(1)}(\omega) = \mathbb{E}\left[\frac{\mathbf{H}_{d_m}(\omega, \theta) - \mathbf{H}_{u_m}(\omega, \theta)}{\mathbf{H}_{u_m}(\omega, \theta)} \right] \tag{65}$$

- Mathematical expectation of the difference between measured damage and undamaged FRF's, divided by the mathematical

expectation of the measured undamaged FRF. It can be expressed as,

$$\mathbf{\Lambda}_m^{(2)}(\omega) = \frac{\mathbb{E}[\mathbf{H}_{d_m}(\omega, \theta) - \mathbf{H}_{u_m}(\omega, \theta)]}{\mathbb{E}[\mathbf{H}_{u_m}(\omega, \theta)]} \tag{66}$$

- Mathematical expectation of the measured crack depth, $\mathbb{E}[\alpha(\omega)]$, calculated by,

$$\mathbf{\Lambda}_m^{(3)}(\omega, \theta) = \frac{\mathbf{H}_{d_m}(\omega, \theta) - \mathbf{H}_{u_m}(\omega, \theta)}{\mathbf{H}_{u_m}(\omega, \theta)} \tag{67}$$

using all samples of $\mathbf{H}_{d_m}(\omega, \theta)$ and $\mathbf{H}_{u_m}(\omega, \theta)$ generated by the stochastic process.

These three ways to calculate the statistics for crack depth and position are used because this is a non-linear problem. Thus, different results are expected for each formulation. An example of that non-linearity will be illustrated in Section 4.2, where these results change as a function of the frequency. Nevertheless, physical crack parameters remain single values. Considering these, the formulations were modified by integrating the measured FRF relative change ($\mathbf{\Lambda}_m$) over the frequency to estimate a single value for α and L_1. By integrating the Eqs. (65)–(67) it has,

$$\overline{\Lambda}_m^{(1)} = \int_\omega \mathbb{E}\left[\frac{\mathbf{H}_{d_m}(\omega, \theta) - \mathbf{H}_{u_m}(\omega, \theta)}{\mathbf{H}_{u_m}(\omega, \theta)}\right] d\omega \tag{68}$$

$$\overline{\Lambda}_m^{(2)} = \int_\omega \frac{\mathbb{E}[\mathbf{H}_{d_m}(\omega, \theta) - \mathbf{H}_{u_m}(\omega, \theta)]}{\mathrm{E}[\mathbf{H}_{u_m}(\omega, \theta)]} d\omega \tag{69}$$

and the third is obtained as $\int_\omega \mathbb{E}[\alpha(\omega)]d\omega$, which is the integral of the mathematical expectation of the measured crack depth, $\mathbb{E}[\alpha(\omega)]$, calculated by,

$$\overline{\Lambda}_m^{(3)}(\omega, \theta) = \frac{\mathbf{H}_{d_m}(\omega, \theta) - \mathbf{H}_{u_m}(\omega, \theta)}{\mathbf{H}_{u_m}(\theta)} \tag{70}$$

Next section shows simulated cases to verify the efficiency of present study.

4. Numerical tests

The system consists of a free-free rod modelled with a two nodes spectral element. It is excited by a unit longitudinal harmonic force applied at the rod element node 1, and the response is obtained at node 2 (Fig. 2). Geometries and material properties are: L=1.0 m, h=0.018 m, b=0.006 m, E=71.0 GPa, η=0.01, and ρ=2700 kg/m^3.

4.1. Deterministic damage detection

To verify the crack depth analytical expression (Eq. (63)), a measured FRF relative change (Eq. (59)) is obtained using the damage model with the crack flexibility (Eq. (56)), then substituted in the Eq. (63). For numerical tests the nominal crack depth values are $\alpha_{no} = \{0.02, 0.10, 0.30\}$, at nominal crack position value $L_1 = 0.35L$. By introducing $\mathbf{\Lambda}_m$ in Eq. (63), the crack depth (α) is estimated. Fig. 5 shows nominal and estimated crack depth with the corresponding percent relative error (Eq. (65)).

Fig. 5 show very good approximation between crack depth nominal and estimated using the approximated equation of crack flexibility (first term of Eq. (56)), provided that the limit of $\alpha \leq 0.13$ be respected (Fig. 4). This is confirmed with the case where nominal crack depth ($\alpha_{no} = 0.30$) extrapolates this limit and $\varepsilon_\alpha = 21.0\%$. In spite of the fact that a crack depth equal to 30% cross-section height is quite considerable size, this approximation is still able to estimate the crack depth with 21.0% error, which from engineering point of view is acceptable. Although not verified here, better crack depth estimation should be expected increasing the polynomial degree of crack flexibility, but at the expenses of an explicit equation of crack depth more complex and difficult to obtain.

Crack position explicit expression (Eq. (64)) is also verified using the same measured FRF relative change for a nominal crack depth value $\alpha_{no} = 0.02$ at the crack position values $L_1^{no} = \{0.33L, 0.63L, 0.85L\}$. By introducing $\mathbf{\Lambda}_m$ in Eq. (64) the crack positions are estimated. Fig. 6 shows the estimated crack position with the corresponding percent relative errors (Eq. (65)).

The results show that the estimation errors for L_1 are very small and with almost the same value for all positions. Although not shown here, others values for α_{no} were tested and for all cases the estimation errors are almost coincident. These results demonstrate that approximations applied to obtain the explicit crack position equation (Eq. (64)) represents a very small change related to the exact solution.

Regards to the uncertainty sources that a structure can contain, the following sections will be dedicated to verifying the efficiency of the present technique for damage detection considering a stochastic system.

4.2. Stochastic damage detection

To start with a numerical test crack depth estimation are considered stochastic dynamic responses for the undamaged and

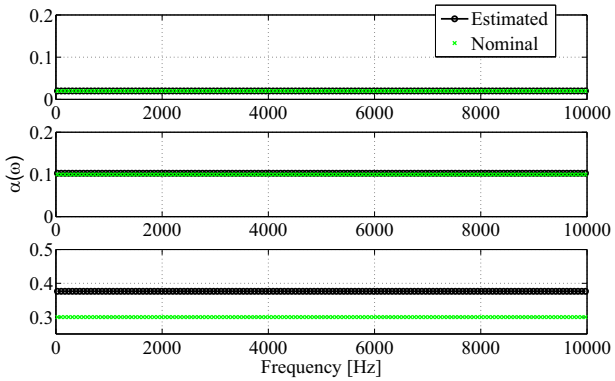

Fig. 5. Crack depth estimated (α) and nominal values ($\alpha_{no} = \{0.02, 0.10, 0.30\}$) at position $L_1 = 0.35L$ with corresponding percent relative errors $\epsilon_\alpha = \{0.1, 2.7, 21.0\}$, respectively.

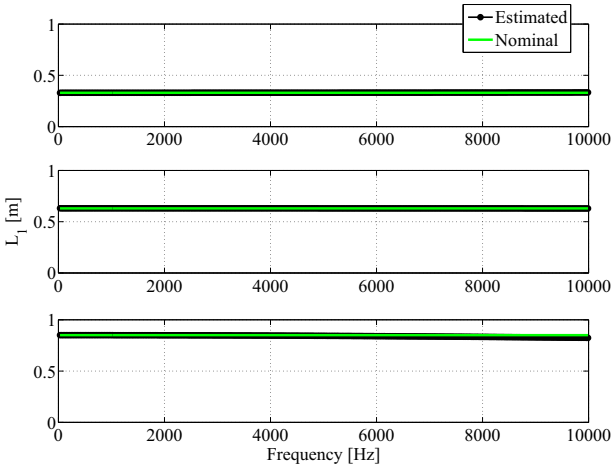

Fig. 6. Crack position estimation (L_1) and nominal values ($L_1^{no} = \{0.33L, 0.63L, 0.85L\}$) for $\alpha_{no} = 0.02$ with corresponding percent relative errors $\epsilon_{L_1} = \{0.24, 0.25, 0.25\}$, respectively.

damage models. Nominal crack depth value is $\alpha_{no} = 0.10$, crack position is $L_1 = 0.3L$ and rod length is L=0.332 m. Variability will be considered for cross section area, Young's modulus and mass density. For the random variable (RV) cases, they are assumed as Gamma distribution with averages: $\mu_A = 0.00096\ \text{m}^2$; $\mu_\rho = 2700\ \text{kg/m}^3$; and $\mu_E = 71.0$ GPa. Coefficient of variation are given by $COV_A = COV_\rho = COV_E = \{0.01, 0.05, 0.1\}$. Monte Carlo simulation is evaluated with 500 samples. For the random field (RF) cases, the longitudinal rigidity $EA(x, \theta)$ and mass per unit length $\rho A(x, \theta)$ have Gamma distribution. The covariance functions are exponential with correlation length b = L/3 and 4 modes. The averages of measured FRF relative change (Eqs. (65)–(67)) are calculated using, $\mathbf{H}_{d_m}(\omega, \theta) = [\mathbf{D}_d(\omega, \theta)]^{-1}$ and $\mathbf{H}_{u_m}(\omega, \theta) = [\mathbf{D}(\omega, \theta)]^{-1}$.

Fig. 7 shows the mean and standard deviation receptance FRFs for an undamaged rod, modelled as deterministic and random variables (RV) with damping factors $\eta = \{0.01, 0.05\}$ and $COV = \{0.01, 0.05, 0.1\}$. Fig. 8 shows the mean and standard deviation receptance FRF's for an undamaged rod, modelled as deterministic and random field (RF) with the same ηs and COVs.

For RV and RF cases, mean responses are slightly different of deterministic response. As the frequency and coefficient of variation increase, the stochastic responses presents an increasing damping behaviour. It comes from the average process which flattens curve peaks as the dispersion increases. These results agree with those presented in [66].

Fig. 9 shows the mean and standard deviation receptance FRFs for the damaged rod, modelled as random variables RV with damping factors $\eta = \{0.01, 0.05\}$ and $COV = \{0.01, 0.05, 0.1\}$. Fig. 10 shows the mean and standard deviation receptance FRFs for the damaged rod, modelled as random variables (RF) with the same ηs and COVs. From this results it can be seen that damaged rod model present similar behaviour as that for the undamaged model.

4.2.1. Crack estimation using random variables

By using the same numerical example, material property and geometry, parameters variability, number of samples and measured FRF relative change as in the Section 4.2, the crack depth (α) is calculated using RV model with $\mathbf{\Lambda}_m^{(1)}$, $\mathbf{\Lambda}_m^{(2)}$, and $\mathbf{\Lambda}_m^{(3)}$ (Eqs. (65)–(67)). By evaluating the structural damping effects on the stochastic damage quantification, two values of damping factor η=0.01 and η=0.05 are used.

Fig. 11 shows the crack depth nominal value and the averages calculated using random variable (RV) model with $\mathbf{\Lambda}_m^{(1)}$, $\mathbf{\Lambda}_m^{(2)}$, and

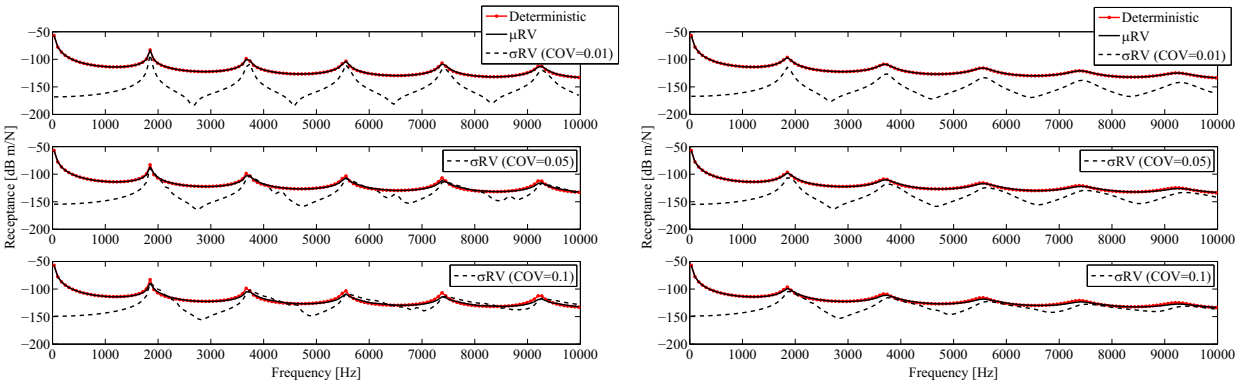

Fig. 7. Mean and standard deviation receptance FRFs ($\mathbf{H}^{12}$) using undamaged rod modelled as deterministic and *RV*, with η=0.01 (LHS) and η=0.05 (RHS) for $COV = \{0.01, 0.05, 0.1\}$.

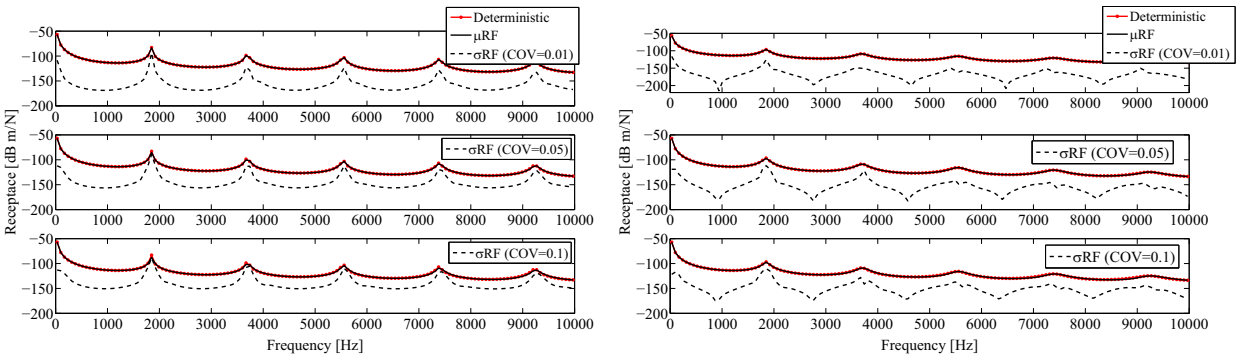

Fig. 8. Mean and standard deviation receptance FRFs ($\mathbf{H}^{12}$) using undamaged rod modelled as deterministic and *RF*, with η=0.01 (LHS) and η=0.05 (RHS) for $COV = \{0.01, 0.05, 0.1\}$.

$\mathbf{\Lambda}_m^{(3)}$ for η=0.01, 0.05 and $COV = \{0.01, 0.05, 0.1\}$.

By considering damping factor η=0.01 (LHS Fig. 11) with the lowest coefficient of variation (COV = 1%), all statistic approaches ($\mathbf{\Lambda}_m^{(1)}$, $\mathbf{\Lambda}_m^{(2)}$, $\mathbf{\Lambda}_m^{(3)}$) present good approximation between estimated and nominal crack depth at some frequency bands. However, at some others frequency bands present low to high dispersion between estimated and nominal crack depth. As the value of *COV* increases the dispersion also increases, where $\mathbf{\Lambda}_\mathbf{m}^{(3)}$ presents higher dispersion as compared to the others. By increasing the damping factor to η=0.05 (RHS Fig. 11), the convergence between estimated and nominal crack depth improves, although it still has moderate dispersion at some frequency bands mainly at high values of *COV*. This comes from the fact that damping greatly influences the behaviour of the stochastic system [67,68].

Fig. 12 shows the crack position nominal value and means obtained using *RV* model with the same statistical approaches, damping factors and coefficient of variation as used before at crack depth analysis. By considering both damping factors η=0.01, 0.05 (LHS and RHS Fig. 12) for all statistical approaches and all values of *COV* very good approximation between nominal and estimated crack position are observed.

The result obtained from *RV* model shows the direct influence of parameters variability into de crack depth estimation error, where as *COV* values increases ε_α increases. Nevertheless, crack position estimation are very close to the nominal value, and the errors are associated mainly with the increasing of *COV* values. Related with the three statistical approaches, $\mathbf{\Lambda}_1(\omega)$ exhibited the best outcome. In general, for all cases, to increase damping factor means to reduce estimation error.

4.2.2. Crack estimation using random field

Consider now that random material properties will change continuously over the structural space. In this situation the dynamic stiffness matrix for the two-node damaged and undamaged rod elements are modelled within the random field framework. By using the same numerical example, parameters variability, number of samples and measured FRF relative change as in the Section 4.2, the crack depth ($\alpha(\omega)$) and crack position ($L_1(\omega)$) are calculated using *RF* model with the statistical approaches $\mathbf{\Lambda}_m^{(1)}$, $\mathbf{\Lambda}_m^{(2)}$, and $\mathbf{\Lambda}_m^{(3)}$ (Eqs. (65)–(67)).

Fig. 13 shows the crack depth nominal value and means calculated using *RF* model with $\mathbf{\Lambda}_m^{(1)}$, $\mathbf{\Lambda}_m^{(2)}$, and $\mathbf{\Lambda}_m^{(3)}$, for $\eta = \{0.01, 0.05\}$ and $COV = \{0.01, 0.05, 0.1\}$. Considering both damping factors $\eta = \{0.01, 0.05\}$ (LHS and RHS Fig. 11), for all statistical approaches ($\mathbf{\Lambda}_\mathbf{m}^{(1)}$, $\mathbf{\Lambda}_\mathbf{m}^{(2)}$, $\mathbf{\Lambda}_\mathbf{m}^{(3)}$) and all values of *COV*, a very large dispersion between estimated crack depth averages and nominal value are observed. As it will be seen later, these results indicates that the proposed statistical approaches are not adequate to obtain a good estimation for crack depth.

Fig. 14 shows crack position nominal value and calculated average using *RF* model with $\mathbf{\Lambda}_m^{(1)}$, $\mathbf{\Lambda}_m^{(2)}$, and $\mathbf{\Lambda}_m^{(3)}$, for $\eta = \{0.01, 0.05\}$ and $COV = \{0.01, 0.05, 0.1\}$. Likewise the crack depth analysis, similar behaviour is observed for the crack position estimation.

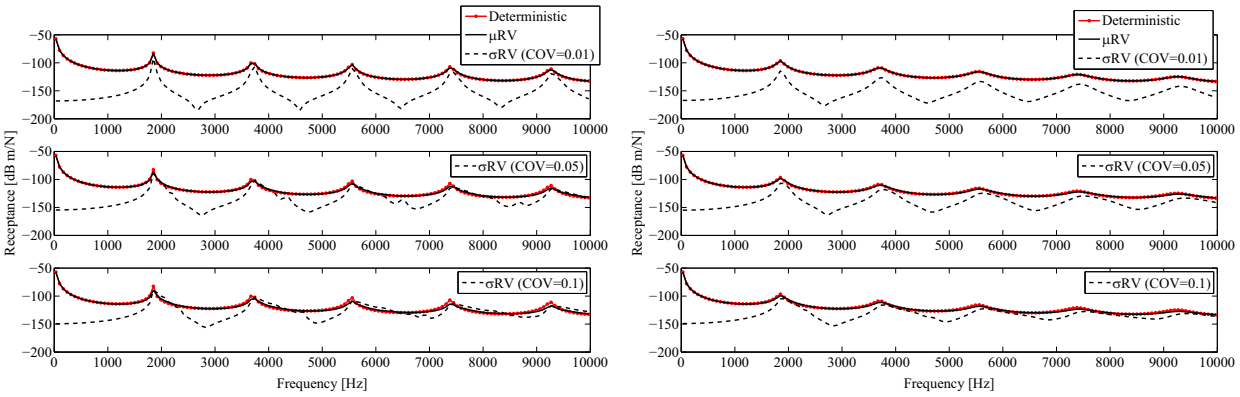

Fig. 9. Mean and standard deviation receptance FRFs ($\mathbf{H}^{12}$) for damaged rod model using *RV* with η=0.01 (LHS) and η=0.05 (RHS) for *COV* = {0.01, 0.05, 0.1}.

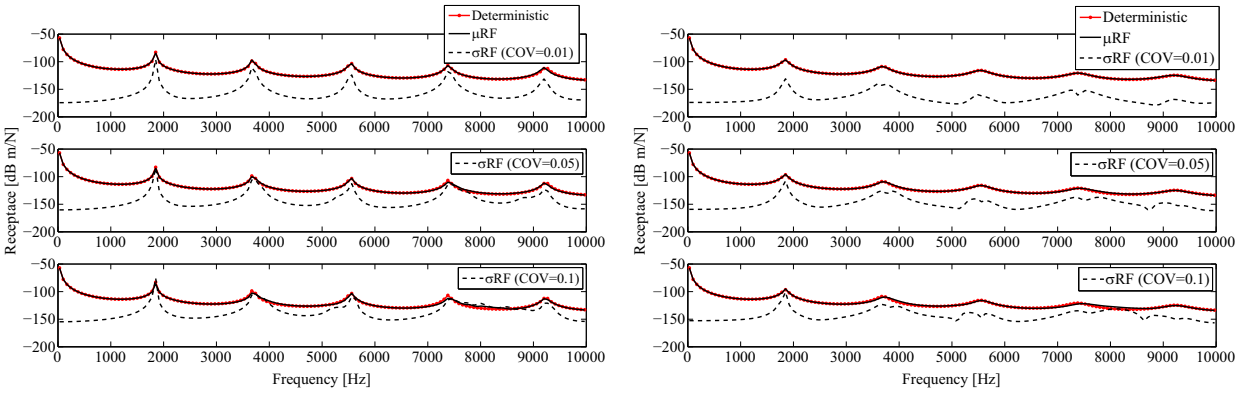

Fig. 10. Mean and standard deviation receptance FRFs ($\mathbf{H}^{12}$) for damaged rod model using *RF* with η=0.01 (LHS) and η=0.05 (RHS) for *COV* = {0.01, 0.05, 0.1}.

Considering both damping factors, all statistical approaches, and all values of *COV*, dispersion between estimated crack position averages and nominal value are smaller than crack depth analysis, but still harmful to obtain its correct estimation. These results reinforce the need for a more adequate statistical approach to estimate crack depth and position.

4.2.3. Crack estimation with integrated measured FRF relative change

To estimate the crack depth and position it is required a measured FRF relative change. Based on stochastic rod models three statistical approaches were proposed initially to obtain the measured FRF relative change (Eqs. (65)–(67)) and applied in the numerical tests. However, as demonstrated in Sections 4.2.1 and 4.2.2, they fail in obtain a single value for the crack depth and position. To overcome this problem, these formulations were modified by integrating the measured FRF relative change over the frequency band of interest (Eqs. (68)–(70)). Using these new approaches the crack depth and position are estimated using stochastic response obtained with *RV* and *RF*. The same numerical example, material property, geometry, parameter variability and number of samples used in Section 4.2, will be applied here.

Table 1 shows crack depth estimated and percent errors obtained using the three new statistical approaches ($\overline{\Lambda}_m^{(1)}$, $\overline{\Lambda}_m^{(2)}$, $\overline{\Lambda}_m^{(3)}$) for η = {0.01, 0.05}, *COV* = {0.01, 0.05, 0.1}. Model parameters are: nominal crack depth α_{no} = 0.10; crack position L_1^{no} = 0.3L; and rod length L=0.332 m. From Table 1 it can be seen that for all values of *COV* with damping factor η=0.01 the calculated crack depths modelled as *RV* present relatively low crack depth errors (ε_α = 2.7–12.0%) as compared with the estimated crack depth modelled as *RF*, where these errors varying from low to very high (ε_α = 2.6–143.7%). As expected, for all cases, ε_α increases as the coefficient of variation increases.

Related with damping factor η=0.05, all *COV*'s and *RV* model the ε_α presents the lowest values (1.6–9.7%), while *RF* model presents similar results as obtained with η=0.01, i.e. the errors varying from low to very high (ε_α = 6.1–112.2%). Nonetheless, some conflicting results have been founded in *RF* model related with *COV*, where for η=0.05 and *COV* = 1% the ε_α increases and for *COV* = 5% and 10% the ε_α decrease as compared with the results obtained with η=0.01. For *RF* model with both damping factor, it can be seen that there are no significant differences between the results obtained with the statistical approaches of $\overline{\Lambda}_1$ and $\overline{\Lambda}_2$. Although the values of ε_α for $\overline{\Lambda}_3$ are higher than the ones of other approaches, they do not present conflicting results for ε_α as *COV* and η changes. Finally, only the results obtained with *RV* model confirms the expected behaviour, where ε_α should increase as *COV* increases, and decreases as η increases.

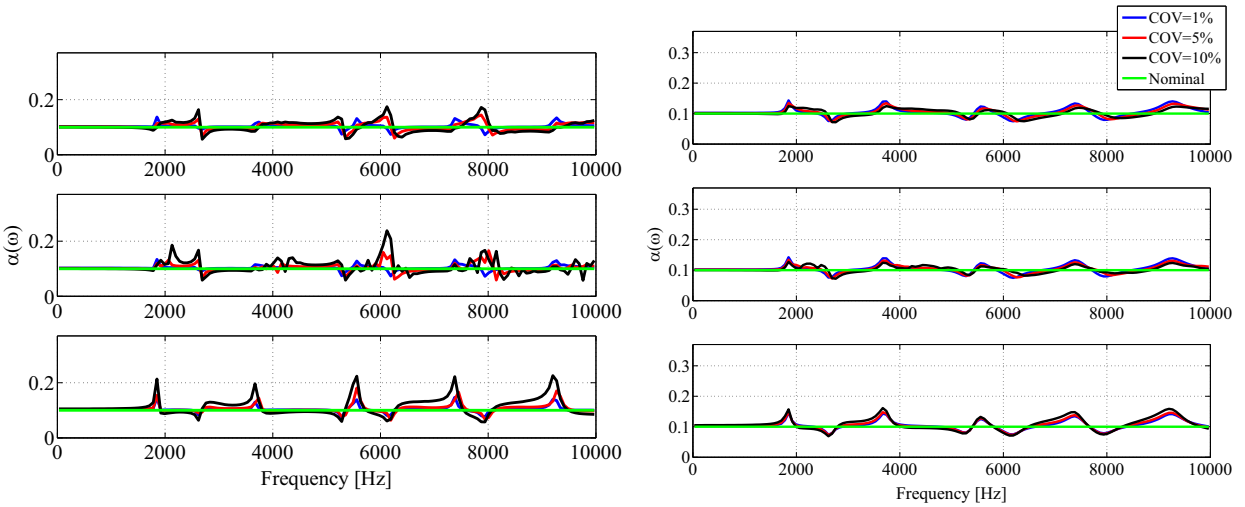

Fig. 11. Crack depth nominal and mean using *RV* model with $\Lambda_{\mathbf{m}}^{(1)}$, $\Lambda_{\mathbf{m}}^{(2)}$, $\Lambda_{\mathbf{m}}^{(3)}$, damping factors η=0.01 (LHS) and η=0.05 (RHS), for $COV = \{0.01, 0.05, 0.1\}$.

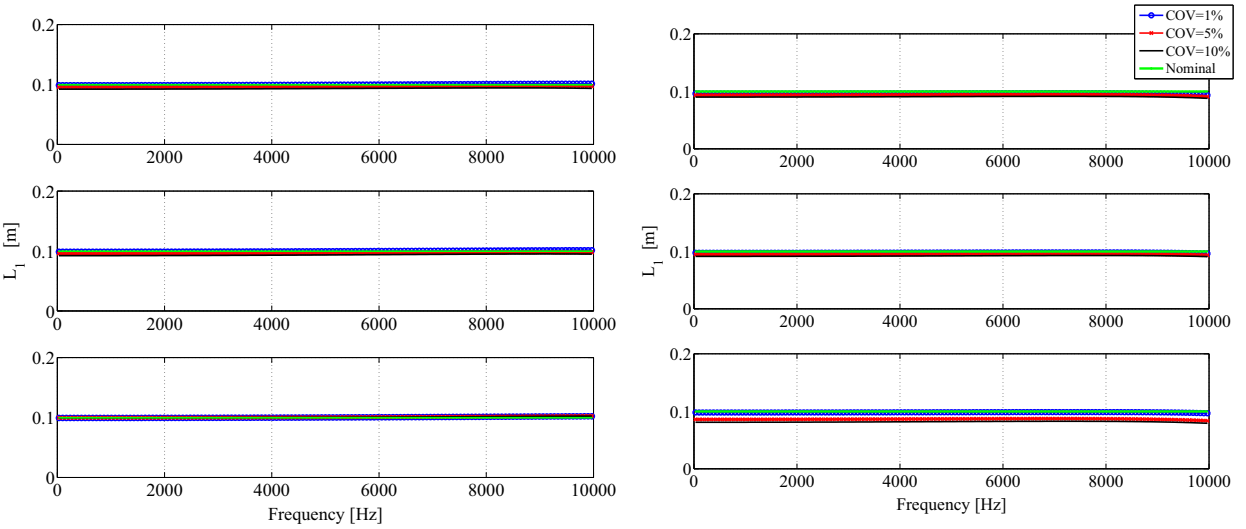

Fig. 12. Crack position nominal and mean using *RV* model with $\Lambda_{\mathbf{m}}^{(1)}$, $\Lambda_{\mathbf{m}}^{(2)}$, $\Lambda_{\mathbf{m}}^{(3)}$, damping factors η=0.01 (LHS) and η=0.05 (RHS), for $COV = \{0.01, 0.05, 0.1\}$.

The crack position and percent error are also evaluated by the three new statistical approaches with the same (η) and (COV) values. Model parameters are the same as the crack depth analysis. Results are presented in Table 2.

From Table 2 it can be seen that The results show that for all cases the crack position was located and the damping factor did not have a great influence in final results. The calculated crack position using the *RV* model presents low error (ε_{L-1} = 0.01–1.9%) for small *COV* and (ε_{L-1} = 5.9–9.9%) for high *COV*. The calculated crack positions using *RF* model had errors between (ε_{L_l} = 1.2–29.8%). In all cases, ε_{L_l} increases as the coefficient of variation increases. Finally, there are no significant differences in the approaches calculated with $\overline{\Lambda}_1$ and $\overline{\Lambda}_2$. The values of ε_{L_l} for $\overline{\Lambda}_3$ are lightly different than the ones of the other approaches but it keeps good results. The results obtained confirms the expected behaviour, where ε_{L_l} should be increasing as *COV* increases.

To summarize, from the damage quantification point of view crack depth estimated using the approach $\overline{\Lambda}_m^{(3)}$ with *RV* model presents good performance. The α estimation using approaches $\overline{\Lambda}_m^{(1)}$ and $\overline{\Lambda}_m^{(2)}$ with *RF* model present some conflicting results as the damping factor increases, which is inconclusive and requires more investigation. The *RF* model fails into estimate crack depth (α) for high values of *COV* independently of the statistical approach used to estimate the measured FRF relative change. Finally, the damage position estimated using the three statistical approaches presents good performance and is able to localize the damage with acceptable errors.

5. Conclusion

A stochastic damage localization and quantification method is presented, which is developed combining Spectral Element Method (SEM) with stochastic approaches where cross-section area, Young's modulus and mass density (A, E, ρ) are modelled as random

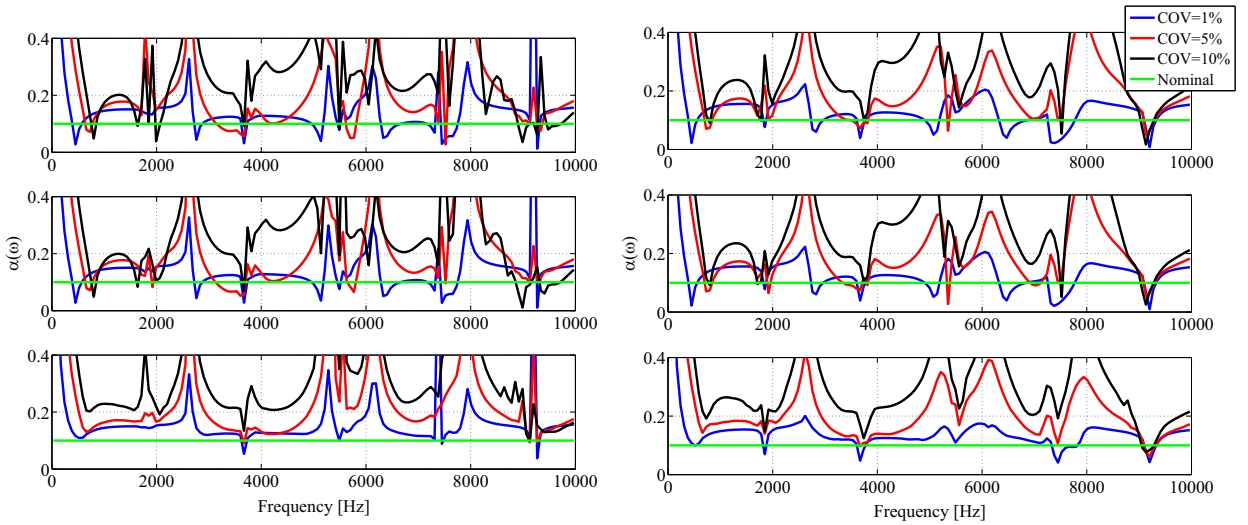

Fig. 13. Crack depth nominal and mean using *RF* model, with $\Lambda_m^{(1)}$, $\Lambda_m^{(2)}$, $\Lambda_m^{(3)}$, damping factors η=0.01 (LHS) and η=0.05 (RHS), for COV = {0.01, 0.05, 0.1}.

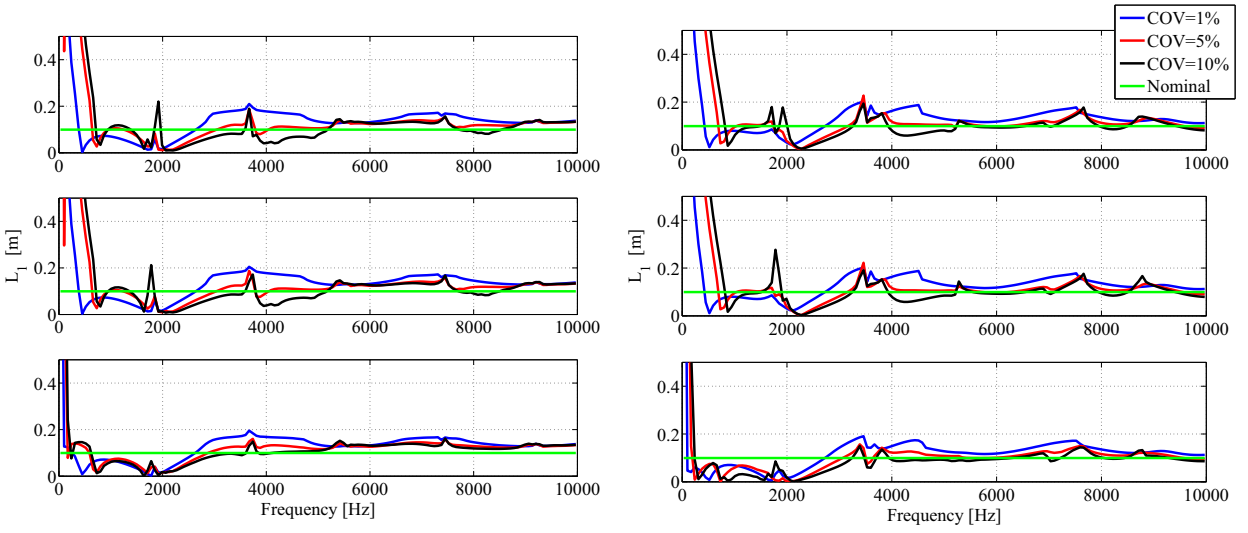

Fig. 14. Crack position nominal and mean using *RF* model, with $\Lambda_m^{(1)}$, $\Lambda_m^{(2)}$, $\Lambda_m^{(3)}$, damping factors η=0.01 (LHS) and η=0.05 (RHS), for COV = {0.01, 0.05, 0.1}.

variables (*RV*) and the spatially distributed longitudinal stiffness (*EA*) and mass per unit length (ρA) are modelled as random field (*RF*). Deterministic formulation for undamaged and damaged rod spectral element, and stochastic undamaged rod spectral element using model parameters as *RV* and *RF* are reviewed and presented. A formulation for stochastic damaged rod spectral element using model parameters as *RV* and *RF* is developed and proposed. The *RF* model is expanded in Karhunen-Loève spectral decomposition using a non-Gaussian distribution obtained from the memoryless non-linear transformation. All stochastic models are solved using Monte Carlo simulation. Numerical tests are conduct using a two nodes rod spectral element in a free-free boundary condition. Stochastic formulations are verified by calculating the mean and standard deviation of receptance FRFs for different *COV*s and compared with deterministic receptance FRFs. Results show very good agreement between stochastic mean and deterministic. As the frequency and *COV* increase the stochastic responses increase damping behaviour. It agrees with [66] and can be explained by the average process which flattens curve peaks as the *COV* values increases, and at lower frequencies the standard deviation is biased by the mean.

An SHM method is proposed where close-form analytical expressions for crack depth (α) and crack position (L_1) estimation are obtained based on measured FRF relative change (Λ_m), calculated with the stochastic damage rod spectral model. Simulated examples are performed using the same two nodes rod spectral element in a free-free boundary condition. Deterministic evaluation between crack depth nominal and estimated using the approximated equation of crack flexibility (Eq. (56)) present a very good approximation, provided that the limit of $\alpha \leq 0.13$ be respected. Similar evaluation for crack position presents negligible errors between nominal and estimated values ($\varepsilon_{L_1} \leq 0.25\%$), for all different positions evaluated. Three initial averages proposed to calculate Λ_m using the stochastic model with *RV* and *RF* presents very high dispersion around nominal values and fails in to estimate crack depth and position. These averages were modified by integrating the former equations over the frequency band and very good

Table 1
Crack depth estimation and percent error using *RV* and *RF* model, with $\overline{\Lambda}_m^{(1)}$, $\overline{\Lambda}_m^{(2)}$, $\overline{\Lambda}_m^{(3)}$, damping factors ($\eta$), and coefficient of variation (*COV*).

	COV	Crack depth (Error ε_α [%])			
	[%]	η=0.01		η=0.05	
		RV	*RF*	*RV*	*RF*
$\overline{\Lambda}_m^{(1)}$	1	0.1027 (2.7)	0.1026 (2.6)	0.1016 (1.6)	0.1061 (6.1)
	5	0.1046 (4.6)	0.1419 (41.0)	0.1018 (1.8)	0.1277 (27.7)
	10	0.1055 (5.5)	0.1890 (89.0)	0.1023 (2.2)	0.1703 (70.3)
$\overline{\Lambda}_m^{(2)}$	1	0.1027 (4.0)	0.1026 (2.6)	0.1023 (2.3)	0.1061 (6.1)
	5	0.1055 (7.0)	0.1419 (41.0)	0.1021 (2.2)	0.1277 (27.7)
	10	0.1134 (11.0)	0.1890 (89.0)	0.1025 (2.5)	0.1703 (70.3)
$\overline{\Lambda}_m^{(3)}$	1	0.1031 (5.0)	0.1077 (7.66)	0.1030 (3.0)	0.1031 (3.05)
	5	0.1084 (11.0)	0.1816 (81.57)	0.1068 (6.8)	0.1588 (58.8)
	10	0.1128 (12.0)	0.2437 (143.7)	0.1097 (9.7)	0.2122 (112.2)

Table 2
Crack position estimation and percent error using *RV* and *RF* model, with $\overline{\Lambda}_m^{(1)}$, $\overline{\Lambda}_m^{(2)}$, $\overline{\Lambda}_m^{(3)}$, damping factors ($\eta$), and coefficient of variation (*COV*).

	COV	Crack position (Error ε_{L_1} [%])			
	[%]	η=0.01		η=0.05	
		RV	*RF*	*RV*	*RF*
$\overline{\Lambda}_m^{(1)}$	1	0.0996 (0.01)	0.0952 (4.4)	0.0976 (1.9)	0.0985 (1.2)
	5	0.0968 (2.8)	0.0869 (12.7)	0.0950 (4.6)	0.0876 (12.1)
	10	0.0968 (5.9)	0.0698 (29.8)	0.0917 (7.9)	0.0702 (29.5)
$\overline{\Lambda}_m^{(2)}$	1	0.0930 (0.016)	0.0965 (3.1)	0.0976 (1.9)	0.0968 (2.8)
	5	0.0997 (2.7)	0.0871 (12.5)	0.0950 (4.6)	0.0881 (11.6)
	10	0.0968 (5.6)	0.0699 (29.8)	0.0919 (7.7)	0.0702 (29.5)
$\overline{\Lambda}_m^{(3)}$	1	0.0933 (0.77)	0.0109 (9.5)	0.0979 (1.7)	0.010 (9.2)
	5	0.10 (0.45)	0.0115 (15.6)	0.0937 (5.9)	0.011 (14.7)
	10	0.0968 (7.77)	0.0128 (28.7)	0.0897 (9.9)	0.012 (24.7)

estimation for crack depth and position using *RV* were findings. However, *RF* model reveals to be unable in find out a reasonable result for α and L_1, independently of the average used to calculate de measured FRF relative change.

Appendix A. Stochastic undamaged rod matrix elements

$$
\begin{aligned}
Ko_{11} &= -\frac{e^{2ikL}k^2(2e^{2ikL}ik\mathrm{wjcos(wjxe)} - 2\mathrm{ikwjcos(wj(L + xe))} + (4\mathrm{k}^2 - (1 + \mathrm{e}^{2ikL})\mathrm{wj}^2)\mathrm{sin(wjxe)} + 2(\mathrm{wj}^2 - 2\mathrm{k}^2)\mathrm{sin(wj(L + xe))})}{(-1 + e^{2ikL})^2(\mathrm{wj}^3 - 4k^2\mathrm{wj})}Ko_{12} \\
&= -\frac{k^2(e^{2ikL}(2ik\,\mathrm{wjcos(wj}(L + \mathrm{xe})) + (4k^2 - \mathrm{wj}^2)\mathrm{sin(wjxe)} + 2(\mathrm{wj}^2 - 2k^2)\mathrm{sin(wj}(L + \mathrm{xe}))) - \mathrm{wj}(2ik\mathrm{cos(wjxe)} + \mathrm{wjsin(wjxe)}))}{(-1 + e^{2ikL})^2(\mathrm{wj}^3 - 4k^2\mathrm{wj})}Ko_{21} \\
&= Ko_{12}Ko_{22} - \frac{e^{2ikL}k^2(-2ik\,\mathrm{wjcos(wjxe)} + 2e^{2ikL}ik\,\mathrm{wjcos(wj}(L + \mathrm{xe})) + 2(2k^2 - \mathrm{wj}^2)\mathrm{sin(wjxe)} - (4k^2 - (1 + e^{2ikL})\mathrm{wj}^2)\mathrm{sin(wj}(L + \mathrm{xe})))}{(-1 + e^{2ikL})^2(\mathrm{wj}^3 - 4k^2\mathrm{wj})}
\end{aligned}
\tag{A.1}
$$

$$
\begin{aligned}
Mo_{11} &= \frac{e^{2ikL}(4\sin(\mathrm{wj}(L+\mathrm{xe}))k^2 + 2e^{2ikL}i\mathrm{wj}\cos(\mathrm{wjxe})k - 2i\mathrm{wj}\cos(\mathrm{wj}(L+\mathrm{xe}))k - (4k^2 + (-1+e^{2ikL})\mathrm{wj}^2)\sin(\mathrm{wjxe}))}{(-1+e^{2ikL})^2(\mathrm{wj}^3 - 4k^2\mathrm{wj})} Mo_{12} \\
&= \frac{e^{2ikL}(4\sin(\mathrm{wj}(L+\mathrm{xe}))k^2 + 2i\mathrm{wj}\cos(\mathrm{wj}(L+\mathrm{xe}))k + (\mathrm{wj}^2 - 4k^2)\sin(\mathrm{wjxe})) - \mathrm{wj}(2ik\cos(\mathrm{wjxe}) + \mathrm{wj}\sin(\mathrm{wjxe}))}{(-1+e^{2ikL})^2(\mathrm{wj}^3 - 4k^2\mathrm{wj})} Mo_{21} = Mo_{12}Mo_{22} \\
&= \frac{e^{4ikL}\mathrm{wj}(2ik\cos(\mathrm{wj}(L+\mathrm{xe})) + \mathrm{wj}\sin(\mathrm{wj}(L+\mathrm{xe}))) - e^{2ikL}(4\sin(\mathrm{wjxe})k^2 + 2i\mathrm{wj}\cos(\mathrm{wjxe})k + (\mathrm{wj}^2 - 4k^2)\sin(\mathrm{wj}(L+\mathrm{xe})))}{(-1+e^{2ikL})^2(\mathrm{wj}^3 - 4k^2\mathrm{wj})}
\end{aligned} \tag{A.2}
$$

$$
\begin{aligned}
Ke_{11} &= -\frac{e^{2ikL}k^2(((1+e^{2ikL})\mathrm{wj}^2 - 4k^2)\cos(\mathrm{wjxe}) + (4k^2 - 2\mathrm{wj}^2)\cos(\mathrm{wj}(L+\mathrm{xe})) + 2ik\mathrm{wj}(e^{2ikL}\sin(\mathrm{wjxe}) - \sin(\mathrm{wj}(L+\mathrm{xe}))))}{(-1+e^{2ikL})^2(\mathrm{wj}^3 - 4k^2\mathrm{wj})} Ke_{12} \\
&= -\frac{k^2(\mathrm{wj}(\mathrm{wj}\cos(\mathrm{wjxe}) - 2ik\sin(\mathrm{wjxe})) + e^{2ikL}((\mathrm{wj}^2 - 4k^2)\cos(\mathrm{wjxe}) + (4k^2 - 2\mathrm{wj}^2)\cos(\mathrm{wj}(L+\mathrm{xe})) + 2ik\,\mathrm{wj}\sin(\mathrm{wj}(L+\mathrm{xe}))))}{(-1+e^{2ikL})^2(\mathrm{wj}^3 - 4k^2\mathrm{wj})} Ke_{21} = Ke_{12}Ke_{22} \\
&= -\frac{e^{2ikL}k^2(2(\mathrm{wj}^2 - 2k^2)\cos(\mathrm{wjxe}) + (4k^2 - (1+e^{2ikL})\mathrm{wj}^2)\cos(\mathrm{wj}(L+\mathrm{xe})) - 2ik\mathrm{wj}(\sin(\mathrm{wjxe}) - e^{2ikL}\sin(\mathrm{wj}(L+\mathrm{xe}))))}{(-1+e^{2ikL})^2(\mathrm{wj}^3 - 4k^2\mathrm{wj})}
\end{aligned} \tag{A.3}
$$

$$
\begin{aligned}
Me_{11} &= \frac{e^{2ikL}((4k^2 + (-1+e^{2ikL})\mathrm{wj}^2)\cos(\mathrm{wjxe}) + 2ik(2ik\cos(\mathrm{wj}(L+\mathrm{xe})) + e^{2ikL}\mathrm{wj}\sin(\mathrm{wjxe}) - \mathrm{wj}\sin(\mathrm{wj}(L+\mathrm{xe}))))}{(-1+e^{2ikL})^2(\mathrm{wj}^3 - 4k^2\mathrm{wj})} Me_{12} \\
&= \frac{\mathrm{wj}(\mathrm{wj}\cos(\mathrm{wjxe}) - 2ik\sin(\mathrm{wjxe})) + e^{2ikL}(-4\cos(\mathrm{wj}(L+\mathrm{xe}))k^2 + 2i\mathrm{wj}\sin(\mathrm{wj}(L+\mathrm{xe}))k + (4k^2 - \mathrm{wj}^2)\cos(\mathrm{wjxe}))}{(-1+e^{2ikL})^2(\mathrm{wj}^3 - 4k^2\mathrm{wj})} Me_{21} = Me_{12}Me_{22} \\
&= \frac{e^{2ikL}(4\cos(\mathrm{wjxe})k^2 - 2i\mathrm{wj}(\sin(\mathrm{wjxe}) - e^{2ikL}\sin(\mathrm{wj}(L+\mathrm{xe})))k + (-4k^2 - e^{2ikL}\mathrm{wj}^2 + \mathrm{wj}^2)\cos(\mathrm{wj}(L+\mathrm{xe})))}{(-1+e^{2ikL})^2(\mathrm{wj}^3 - 4k^2\mathrm{wj})}
\end{aligned} \tag{A.4}
$$

Appendix B. Damaged rod matrix elements

B.1. Deterministic

$$
\begin{aligned}
K_{0d_{11}} &= EAk\{[4(k(\Theta(k^2L_1\Theta - 1) + 2L) + \sin(2kL)) + k\Theta(4(k^2L_1\Theta - 1)\cos(2k(L - L_1)) + k(\Theta(\sin(2k(L - 2L_1)) - \sin(2kL) - 2\sin(2kL_1)) \\
&\quad + 8L_1\sin(2k(L - L_1))) + 4\cos(2kL) + 4\cos(2kL_1))]/[4(k\Theta(\cos(k(L - 2L_1)) + \cos(kL)) + 2\sin(kL))^2]\}K_{0d_{12}} \\
&= EAk\left\{\frac{(k^2\Theta(L - 2L_1)\sin(k(L - 2L_1)) + (k^2L\Theta - 2)\sin(kL) - 2kL\cos(kL))}{(k\Theta(\cos(k(L - 2L_1)) + \cos(kL)) + 2\sin(kL))^2}\right\}K_{0d_{21}} = K_{0d_{12}}K_{0d_{22}} \\
&= EAk\{[4(k^3\Theta^2(L - L_1) + 2kL + \sin(2kL) - k\Theta) + k\Theta(4\cos(2kL_1)(k^2\Theta(L - L_1) - 1) - k\Theta(\sin(2k(L - 2L_1)) + 2\sin(2k(L - L_1)) + \sin(2kL)) \\
&\quad + 8k(L - L_1)\sin(2kL_1) + 4\cos(2k(L - L_1)) + 4\cos(2kL))]/[4(k\Theta(\cos(k(L - 2L_1)) + \cos(kL)) + 2\sin(kL))^2]\}
\end{aligned} \tag{B.1}
$$

$$
\begin{aligned}
M_{0d_{11}} &= \rho A\{[4k(k^2L_1\Theta^2 + \Theta + 2L) - 4\sin(2kL) + k\Theta(-4\cos(2kL) + 4(L_1\Theta k^2 + 1)\cos(2k(L - L_1)) - 4\cos(2kL_1) + 8kL_1\sin(2k(L - L_1)) \\
&\quad + k\Theta(\sin(2kL) - \sin(2k(L - 2L_1)) + 2\sin(2kL_1)))]/[4k(k\Theta(\cos(kL) + \cos(k(L - 2L_1))) + 2\sin(kL))^2]\}M_{0d_{12}} \\
&= \rho A\left\{\frac{(L - 2L_1)\Theta\sin(k(L - 2L_1))k^2 - 2L\cos(kL)k + (L\Theta k^2 + 2)\sin(kL)}{k(k\Theta(\cos(kL) + \cos(k(L - 2L_1))) + 2\sin(kL))^2}\right\}M_{0d_{21}} = M_{0d_{12}}M_{0d_{22}} \\
&= \rho A\{[4k(k^2(L - L_1)\Theta^2 + \Theta + 2L) - 4\sin(2kL) + k\Theta(-4\cos(2kL) - 4\cos(2k(L - L_1)) + 4((L - L_1)\Theta k^2 + 1)\cos(2kL_1) \\
&\quad + k\Theta(\sin(2kL) + \sin(2k(L - 2L_1)) + 2\sin(2k(L - L_1))) + 8k(L - L_1)\sin(2kL_1))]/[4k(k\Theta(\cos(kL) + \cos(k(L - 2L_1))) + 2\sin(kL))^2]\}
\end{aligned} \tag{B.2}
$$

B.2. Stochastic

$$
\begin{aligned}
SkLo_{11} &= -\frac{k^2(-2ik\cos(\mathrm{wjxe}) + 2e^{-2ikL_1}ik\cos(\mathrm{wj}(L_1 + \mathrm{xe})) + \mathrm{wj}\sin(\mathrm{wjxe}) - e^{-2ikL_1}\mathrm{wj}\sin(\mathrm{wj}(L_1 + \mathrm{xe})))}{4k^2 - \mathrm{wj}^2} SkLo_{12} = \frac{e^{-ikL_1}k^2(\sin(\mathrm{wj}(L_1 + \mathrm{xe})) - \sin(\mathrm{wjxe}))}{\mathrm{wj}} \\
SkLo_{21} &= SkLo_{12}; \quad SkLo_{22} = -\frac{k^2(2e^{-2ikL_1}ik\cos(\mathrm{wjxe}) - 2ik\cos(\mathrm{wj}(L_1 + \mathrm{xe})) + e^{-2ikL_1}\mathrm{wj}\sin(\mathrm{wjxe}) - \mathrm{wj}\sin(\mathrm{wj}(L_1 + \mathrm{xe})))}{4k^2 - \mathrm{wj}^2}
\end{aligned}
$$

$$
\begin{aligned}
SmLo_{11} &= \frac{-2ik\cos(\mathrm{wjxe}) + \mathrm{wj}\sin(\mathrm{wjxe}) + e^{-2ikL_1}(2ik\cos(\mathrm{wj}(L_1 + \mathrm{xe})) - \mathrm{wj}\sin(\mathrm{wj}(L_1 + \mathrm{xe})))}{4k^2 - \mathrm{wj}^2} SmLo_{12} = \frac{e^{-ikL_1}(\sin(\mathrm{wj}(L_1 + \mathrm{xe})) - \sin(\mathrm{wjxe}))}{\mathrm{wj}} SmLo_{21} \\
&= SmLo_{12}; \quad SmLo_{22} = \frac{-2ik\cos(\mathrm{wj}(L_1 + \mathrm{xe})) + e^{-2ikL_1}(2ik\cos(\mathrm{wjxe}) + \mathrm{wj}\sin(\mathrm{wjxe})) - \mathrm{wj}\sin(\mathrm{wj}(L_1 + \mathrm{xe}))}{4k^2 - \mathrm{wj}^2}
\end{aligned}
$$

$$SkRo_{11} = -\frac{k^2(e^{-2ikL_1}(\mathrm{wjsin(wjxe)} - 2ik\mathrm{cos(wjxe)}) + e^{-2ikL}(2ik\mathrm{cos(wj}(L - L_1 + \mathrm{xe})) - \mathrm{wjsin(wj}(L - L_1 + \mathrm{xe}))))}{4k^2 - \mathrm{wj}^2} SkRo_{12}$$

$$= \frac{e^{-ikL}k^2(\mathrm{sin(wj}(L - L_1 + \mathrm{xe})) - \mathrm{sin(wjxe)})}{\mathrm{wj}} SkRo_{21} = SkRo_{12};$$

$$SkRo_{22} = \frac{k^2(2ik\mathrm{cos(wj}(L - L_1 + \mathrm{xe})) - ie^{2ik(L_1 - L)}(2k\mathrm{cos(wjxe)} - i\mathrm{wjsin(wjxe)}) + \mathrm{wjsin(wj}(L - L_1 + \mathrm{xe})))}{4k^2 - \mathrm{wj}^2}$$

$$SmRo_{11} = \frac{e^{-2ikL_1}(\mathrm{wjsin(wjxe)} - 2ik\mathrm{cos(wjxe)}) + e^{-2ikL}(2ik\mathrm{cos(wj}(L - L_1 + \mathrm{xe})) - \mathrm{wjsin(wj}(L - L_1 + \mathrm{xe})))}{4k^2 - \mathrm{wj}^2} SmRo_{12}$$

$$= \frac{e^{-ikL}(\mathrm{sin(wj}(L - L_1 + \mathrm{xe})) - \mathrm{sin(wjxe)})}{\mathrm{wj}} SmRo_{21} = SmRo_{12};$$

$$SmRo_{22} = \frac{-2ik\mathrm{cos(wj}(L - L_1 + \mathrm{xe})) + e^{2ik(L_1 - L)}(2ik\mathrm{cos(wjxe)} + \mathrm{wjsin(wjxe)}) - \mathrm{wjsin(wj}(L - L_1 + \mathrm{xe}))}{4k^2 - \mathrm{wj}^2}$$

$$SkLe_{11} = -\frac{k^2(-\mathrm{wjcos(wjxe)} + e^{-2ikL_1}\mathrm{wjcos(wj}(L_1 + \mathrm{xe})) - 2ik\mathrm{sin(wjxe)} + 2e^{-2ikL_1}ik\mathrm{sin(wj}(L_1 + \mathrm{xe})))}{4k^2 - \mathrm{wj}^2} SkLe_{12}$$

$$= \frac{e^{-ikL_1}k^2(\mathrm{cos(wjxe)} - \mathrm{cos(wj}(L_1 + \mathrm{xe})))}{\mathrm{wj}} SkLe_{21} = SkLe_{12};$$

$$SkLe_{22} = -\frac{k^2(-e^{-2ikL_1}\mathrm{wjcos(wjxe)} + \mathrm{wjcos(wj}(L_1 + \mathrm{xe})) + 2ik(e^{-2ikL_1}\mathrm{sin(wjxe)} - \mathrm{sin(wj}(L_1 + \mathrm{xe}))))}{4k^2 - \mathrm{wj}^2}$$

$$SmLe_{11} = \frac{-\mathrm{wjcos(wjxe)} - 2ik\mathrm{sin(wjxe)} + e^{-2ikL_1}(\mathrm{wjcos(wj}(L_1 + \mathrm{xe})) + 2ik\mathrm{sin(wj}(L_1 + \mathrm{xe})))}{4k^2 - \mathrm{wj}^2} SmLe_{12}$$

$$= + \frac{e^{-ikL_1}(\mathrm{cos(wjxe)} - \mathrm{cos(wj}(L_1 + \mathrm{xe})))}{\mathrm{wj}} SME_{21}^1 = SME_{12}^1;$$

$$SmLe_{22} = \frac{\mathrm{wjcos(wj}(L_1 + \mathrm{xe})) + e^{-2ikL_1}(2ik\mathrm{sin(wjxe)} - \mathrm{wjcos(wjxe)}) - 2ik\mathrm{sin(wj}(L_1 + \mathrm{xe}))}{4k^2 - \mathrm{wj}^2}$$

$$SkRe_{11} = -\frac{k^2(e^{-2ikL}(\mathrm{wjcos(wj}(L - L_1 + \mathrm{xe})) + 2ik\mathrm{sin(wj}(L - L_1 + \mathrm{xe}))) - e^{-2ikL_1}(\mathrm{wjcos(wjxe)} + 2ik\mathrm{sin(wjxe)}))}{4k^2 - \mathrm{wj}^2} SkRe_{12}$$

$$= \frac{e^{-ikL}k^2(\mathrm{cos(wjxe)} - \mathrm{cos(wj}(L - L_1 + \mathrm{xe})))}{\mathrm{wj}} SkRe_{21} = SkRe_{12};$$

$$SkRe_{22} = \frac{k^2(-\mathrm{wjcos(wj}(L - L_1 + \mathrm{xe})) + e^{2ik(L_1 - L)}(\mathrm{wjcos(wjxe)} - 2ik\mathrm{sin(wjxe)}) + 2ik\mathrm{sin(wj}(L - L_1 + \mathrm{xe})))}{4k^2 - \mathrm{wj}^2}$$

$$SmRe_{11} = \frac{e^{-2ikL}(\mathrm{wjcos(wj}(L - L_1 + \mathrm{xe})) + 2ik\mathrm{sin(wj}(L - L_1 + \mathrm{xe}))) - e^{-2ikL_1}(\mathrm{wjcos(wjxe)} + 2ik\mathrm{sin(wjxe)})}{4k^2 - \mathrm{wj}^2} SmRe_{12}$$

$$= \frac{e^{-ikL}(\mathrm{cos(wjxe)} - \mathrm{cos(wj}(L - L_1 + \mathrm{xe})))}{\mathrm{wj}} SmRe_{21} = SmRe_{12};$$

$$SmRe_{22} = \frac{\mathrm{wjcos(wj}(L - L_1 + \mathrm{xe})) + e^{2ik(L_1 - L)}(2ik\mathrm{sin(wjxe)} - \mathrm{wjcos(wjxe)}) - 2ik\mathrm{sin(wj}(L - L_1 + \mathrm{xe}))}{4k^2 - \mathrm{wj}^2}$$

References

[1] S.W. Doebling, C.R. Farrar, M. Prime, A review of vibration-based damage identification methods, Tech. Rep., Engineering Analysis Group Los Alamos National Laboratory, 1998.

[2] D. Montalvão, N. Maia, A. Ribeiro, A review of vibration-based structural health monitoring with special emphasis on composite materials, Shock Vib. Dig. 38 (2006) 295–324.

[3] M. Krawczuk, J. Grabowska, M. Palacz, Longitudinal wave propagation. Part I - Comparison of rod theories, J. Sound Vib. 295 (2006) 461–478. http://dx.doi.org/10.1016/j.jsv.2005.12.048.

[4] M. Krawczuk, Application of spectral beam finite element with a crack and iterative search technique for damage detection, Finite Elem. Anal. Des. 80 (2002) 1809–1816. http://dx.doi.org/10.1016/S0168-874X(01)00084-1.

[5] W.M. Ostachowicz, Damage detection of structures using spectral finite element method, Comput. Struct. 86 (2008) 454–462. http://dx.doi.org/10.1016/j.compstruc.2007.02.004.

[6] Z. Su, L. Ye, Identification of Damage Using Lamb Waves, Springer, Berlin, 2009.

[7] E. Santos, J. Arruda, J.D. Santos, Modeling of coupled structural systems by an energy spectral element method, J. Sound Vib. 36 (2008) 1–24.

[8] J.F. Doyle, Wave Propagation in Structures: spectral Analysis using Fast Discrete Fourier Transforms, Mechanical Engineering, 2nd edition, Springer-Verlag, Inc., New York, New York, 1997.
[9] U. Lee, Spectral element method in structural dynamics, BInha Univ. Press (2004).
[10] M. Paz, Structural Dynamics: Theory and Computation, 2nd edition, Van Nostrand, Reinhold, US, 1980.
[11] J.R. Banerjee, F.W. Williams, Exact bernoulli-euler dynamic stiffness matrix for a range of tapered beams, Int. J. Numer. Methods Eng. 21 (12) (1985) 2289–2302.
[12] J.R. Banerjee, Coupled bending torsional dynamic stiffness matrix for beam elements, Int. J. Numer. Methods Eng. 28 (6) (1989) 1283–1298.
[13] J.R. Banerjee, F.W. Williams, Coupled bending-torsional dynamic stiffness matrix for timoshenko beam elements, Comput. Struct. 42 (3) (1992) 301–310.
[14] J.R. Banerjee, S.A. Fisher, Coupled bending torsional dynamic stiffness matrix for axially loaded beam elements, Int. J. Numer. Methods Eng. 33 (4) (1992) 739–751.
[15] N.J. Ferguson, W.D. Pilkey, Literature review of variants of dynamic stiffness method, Part 1: the dynamic element method, Shock Vib. Dig. 25 (2) (1993) 3–12.
[16] N.J. Ferguson, W.D. Pilkey, Literature review of variants of dynamic stiffness method, Part 2: frequency-dependent matrix and other, Shock Vib. Dig. 25 (4) (1993) 3–10.
[17] J.R. Banerjee, F.W. Williams, Free-vibration of composite beams – an exact method using symbolic computation, J. Aircr. 32 (3) (1995) 636–642.
[18] C.S. Manohar, S. Adhikari, Dynamic stiffness of randomly parametered beams, Probabilistic Eng. Mech. 13 (1) (1998) 39–51.
[19] J.R. Banerjee, Dynamic stiffness formulation for structural elements: a general approach, Comput. Struct. 63 (1) (1997) 101–103.
[20] S. Adhikari, C.S. Manohar, Transient dynamics of stochastically parametered beams, ASCE J. Eng. Mech. 126 (11) (2000) 1131–1140.
[21] J.F. Doyle, Wave Propagation in Structures, Springer Verlag, New York, 1989.
[22] S. Gopalakrishnan, A. Chakraborty, D.R. Mahapatra, Spectral Finite Element Method, Springer Verlag, New York, 2007.
[23] S.M. Hashemi, M.J. Richard, G. Dhatt, A new Dynamic Finite Element (DFE) formulation for lateral free vibrations of Euler-Bernoulli spinning beams using trigonometric shape functions, J. Sound Vib. 220 (4) (1999) 601–624.
[24] S.M. Hashemi, M.J. Richard, Free vibrational analysis of axially loaded bending-torsion coupled beams: a dynamic finite element, Comput. Struct. 77 (6) (2000) 711–724.
[25] M.P.M. Krawczuk, Analysis of longitudinal wave propagation in a cracked rod by the spectral element method, Comput. Struct. 80 (24) (2002) 1809–1816. http://dx.doi.org/10.1016/S0045-7949(02)00219-5.
[26] M.V.V.S. Murthy, S. Gopalakrishnan, P.S. Nair, Signal wrap around free spectral finite element formulation for multiply connected 1d wave guides, J. Aerosp. Sci. Technol. 63 (2011) 72–88.
[27] S. Adhikari, M. Friswell, Distributed parameter model updating using the Karhunen-Loève expansion, Mech. Syst. Signal Process. 24 (2010) 326–339.
[28] V. Ajith, S. Gopalakrishnan, Spectral element approach to wave propagation in uncertain beam structures, J. Mech. Mater. Struct. 5 (4) (2010) 637–659.
[29] A.T. Fabro, T.G. Ritto, R. Sampaio, J.R.F. Arruda, Stochastic analysis of a cracked rod modeled via the spectral element method, Mech. Res. Commun. 37 (2010) 326–331. http://dx.doi.org/10.1016/j.mechrescom.2010.03.005.
[30] C. Ng, M. Veidt, H. Lam, Probabilistic damage characterisation in beams using guided waves, Procedia Eng. 14 (2011) 490–497.
[31] J.C.B.D.E.B. Flynn, M.D. Todd, P. Wilcox, Enhanced detection through low-order stochastic modeling for guided-wave structural health monitoring, Structural Health Monitoring.
[32] M.R. Machado, J.M.C.D. Santos, Reliability analysis of damaged beam spectral element with parameter uncertainties, Shock Vib. 2015 (2015) 12. http://dx.doi.org/10.1155/2015/574846.
[33] C.R. Farrar, K. Worden, An introduction to structural health monitoring, Philos. Trans. R. Soc. 365 (2007) 303–315.
[34] S.W. Doebling, C.R. Farrar, M. Prime, D.W. Shevitz, Damage identification and health monitoring of structural and mechanical systems from changes in their vibration characteristics- a literature review, Tech. Rep., Los Alamos National Laboratory – University of California, 1996.
[35] R.C. Aster, C.H. Thurber, Parameter Estimation and Inverse Problems, Academic Press publications, USA, 2012.
[36] M.I. Friswell, Damage identification using inverse methods, Philos. Trans. R. Soc. 2007 (2007) 393–410.
[37] J.E. Mottershead, M. Friswell, Model updating in strucutral dynamics: a survey, J. Sound Vib. 167 (2) (1993) 347–375.
[38] C. Fritzen, D. Jennewein, Damage detection based on model updating methods, Mech. Syst. Signal Process. 12 (1) (1998) 163–186.
[39] M.I. Friswell, J.E. Mottershead, Finite Element Model Updating in Structural Dynamics, Kluwer Academic Publishers, Dordrecht, The Netherlands, 1995.
[40] A. Morassi, F. Vestroni, Dynamic Methods for Damage Detection in Strucutres, Springer, New York, 2008.
[41] J.M.C. DosSantos, D.C. Zimmerman, Structural damage detection using minimum rank update theory and parameter estimation, in: Proceedings of the AIAA/ASME/AHS Adaptive Structures Forum, 1996.
[42] O.C. Zienkiewicz, R.L. Taylor, The Finite Element Method, Butterworth-Heinemann, Bristol, UK, 2000.
[43] N.M. Maia, M. Julio, Theoretical and Experimental Modal Analysis, Research Studies Press, Baldock, Hertforshire, England, 1997.
[44] Y. Xu, J. Zhang, J. Li, X. Wang, Stochastic damage detection method for building structures with parametric uncertainties, J. Sound Vib. 330 (2011) 4725–4737.
[45] O. ArdaVanli, S. Jung, Statistical updating of finite element model with lamb wave sensing data for damage detection problems, Mechanical Systems and Signal Processing.
[46] H.H. Khodaparast, J. Mottershead, Efficient methods in stochastic model updating, in: Proceedings of the ISMA, 2008.
[47] A. Papoulis, S.U. Pillai, Probability, Random Variables and Stochastic Processes, McGraw-Hill, Boston, 2002.
[48] I.M. Sobol', A Primer for the Monte Carlo Method, CRC Press, USA, 1994.
[49] D. Xiu, Numerical Methods for Computations – a Spectral Method Approcah, Princeton University Press, 2010.
[50] R. Ghanem, P. Spanos, Stochastic Finite Elements – a Spectral Approach, Springer, New York, USA, 1991.
[51] M. Grigoriu, Simulation of stationary non-gaussian translation processes, J. Eng. Mech. 124 (1998) 121–126. http://dx.doi.org/10.1061/(ASCE)0733-9399(1998)124:2(121).
[52] F. Poirion, C. Soize, Monte carlo construction of karhunen-loeve expansion for non-gaussian random fields, in: Proceedings of the 13th ASCE Engineering Mechanics Division Conference, 1999.
[53] R. Vio, P. Andreani, W. Wamsteker, Nmerical simularin of non-gaussian random fields with prescribed correlation structure, Tech. Rep., ESA IUE Obsevatory and Max-Planck Institut fur Extraterrestrische Physik, 2001.
[54] P.F. Puig, B., C. Soize, Non-gaussian simulation using hermite polynomial expansion: convergences and algorithms, Probabilistic Engineering Mechanics, vol. 17(3), 2002, pp. 253–264. ⟨http://dx.doi.org/10.1016/S0266-8920(02)00010-3⟩.
[55] S. Sakamoto, R. Ghanem, Simulation of multi-dimensional non-Gaussian non-stationary random fields, Probabilistic Eng. Mech. 17 (2002) 167–176.
[56] G.L.M. Schevenels, G. Degrande, Application of the stochastic finite element method for gaussian and non-gaussian systems, in: Proceedings of the International Conference on Noise and Vibration Engineering, 2004.
[57] H.H.W. Phoon K.K., S.T. Quek, Simulation of strongly non-gaussian processes using karhunen-loeve expansion, Structural Safety, vol. 20(2), 2005, p. 1881198. ⟨http://dx.doi.org/10.1016/j.probengmech.2005.05.007⟩.
[58] G. Weinberg, L. Gunn, Simulation of statistical distributions using the memoryless nonlinear transformation, Tech. Rep., DSTO Defence Science and Technology Organisation-Australia Government, 2011.
[59] M. Hazewinkel, Encyclopaedia of Mathematics: Fibonacci Method-H, Kluwer Academic Publishers, Dordrecht, The Netherlands, 1989.
[60] D. Xiu, G.E. Karniadakis, The Wiener-Askey polynomial chaos for stochastic differential equations, Tech. Rep., Brown University, Division of Applied Mathematics, 182 George Street, Providence, RI, 2003.
[61] M. Krawczuk, J. Grabowska, M. Palacz, Longitudinal wave propagation. Part II- Analysis of crack influence, J. Sound Vib. 295 (2006) 479–490. http://dx.doi.org/10.1016/j.jsv.2005.12.049.
[62] H. Tada, P. Paris, G.R. Irwin, Stress Analysis of Cracks Handbook, Del Research Corporation, USA, 1973.
[63] J.-J. Sinou, Numerical investigations of a robust identification of crack location and size in beams using only changes in ratio pulsations of the cracked beams,

Struct. Eng. Mech. 25 (6) (2007) 691–716.
[64] Y. Narkis, Identification of crack location in vibrating simply supported beams, J. Sound Vib. 172 (4) (1994) 549–558.
[65] J.-J. Sinou, A Review of damage detection and health monitoring of mechanical systems from changes in the measurement of linear and non-linear vibrations, Tech. Rep., Laboratoire de Tribologie et Dynamique des Systemes UMR-CNRS 5513 Ecole Centrale de Lyon, 2013.
[66] S. Adhikari, Doubly spectral stochastic finite-element method for linear structural dynamics, Am. Soc. Civ. Eng. 1 (2011) 264–276.
[67] R. Pavlovic, P. Kozić, P. Rajković, Influence of randomly varying damping coefficient on the dynamic stability of continuous systems, Eur. J. Mech./A Solids 24 (2005) 81–87.
[68] S. Adhikari, Structural Dynamic Analysis with Generalized Damping Models, Wiley, USA, 2013.